# Reevaluating carbon fluxes in subduction zones, what goes down, mostly comes up

Peter B. Kelemen[a,1] and Craig E. Manning[b,1]

[a]Department of Earth & Environmental Sciences, Columbia University, Lamont–Doherty Earth Observatory, Palisades, NY 10964; and [b]Department of Earth, Planetary, and Space Sciences, University of California, Los Angeles, CA 90095

This contribution is part of the special series of Inaugural Articles by members of the National Academy of Sciences elected in 2014.

Contributed by Peter B. Kelemen, April 23, 2015 (sent for review August 7, 2014; reviewed by Jay J. Ague, James Connolly, Rajdeep Dasgupta, and Dimitri Sverjensky)

**Carbon fluxes in subduction zones can be better constrained by including new estimates of carbon concentration in subducting mantle peridotites, consideration of carbonate solubility in aqueous fluid along subduction geotherms, and diapirism of carbon-bearing metasediments. Whereas previous studies concluded that about half the subducting carbon is returned to the convecting mantle, we find that relatively little carbon may be recycled. If so, input from subduction zones into the overlying plate is larger than output from arc volcanoes plus diffuse venting, and substantial quantities of carbon are stored in the mantle lithosphere and crust. Also, if the subduction zone carbon cycle is nearly closed on time scales of 5–10 Ma, then the carbon content of the mantle lithosphere + crust + ocean + atmosphere must be increasing. Such an increase is consistent with inferences from noble gas data. Carbon in diamonds, which may have been recycled into the convecting mantle, is a small fraction of the global carbon inventory.**

carbon cycle | subduction | aqueous geochemistry | metasediment diapirs | peridotite carbonation

Flux of carbon that is returned to Earth's interior by subduction is important but poorly constrained. There have been several recent reviews of the subduction carbon cycle (1–8). These studies estimate that about half of subducted carbon is removed from the downgoing plate beneath forearcs and arcs and returned to Earth's surface [40% in Gorman et al. (8); 20–80% in Dasgupta and Hirschmann (1); and 18–70% in Johnston et al. (6)].

Key carbon reservoirs and transport mechanisms can now be better quantified. These include carbon concentration ([C]) in altered mantle lithologies (this paper plus refs. 9 and 10), carbon solubility in aqueous fluids at subduction zone conditions (this paper plus refs. 11 and 12), the volume of altered peridotites in subducting oceanic plates (especially ref. 13), the volume of altered peridotite in the mantle wedge, and the nature of metasedimentary diapirs rising from subducting crust (14).

In this paper, we reevaluate carbon fluxes in several tectonic settings. We start with carbon uptake during hydrothermal alteration near midocean ridges, followed by an estimate of carbon addition during alteration of shallow mantle peridotite at the "outer rise," where subducting oceanic plates bend before subduction. We then consider carbon transfer in fluids and melts derived from the subducting plate. Finally, we review carbon outputs from arc volcanoes and via diffuse venting.

## Carbon Uptake During Hydrothermal Alteration of Basaltic Oceanic Crust: 22–29 Mt C/y

Following Alt and Teagle (15), we compiled data on [C] in altered oceanic crust (Dataset S1; also see *SI Text*). [C] is now thought to be higher in volcanic rocks and lower in gabbros. These differences offset each other, so our estimate of 500–600 ppm carbon in oceanic crust agrees with Alt and Teagle. Oceanic plates are consumed at an average of ∼0.05 m/y along the ∼44,500-km length of global subduction zones (4). These values and [C] in altered oceanic crust yield a carbon flux of 22–29 Mt C/y (Dataset S2).

Seismic data and seafloor outcrops imply that 5–15% of oceanic crust that formed at slow- and ultraslow-spreading ridges is composed of altered mantle peridotite, with the extent of serpentinization varying from ∼100% at the seafloor to ∼0% at ∼7 km depth (16, 17). Because slow- and ultraslow-spreading crust is formed at ∼30% of midocean ridges (18, 19), crust composed of altered peridotite is 1–4% of the total, and not a significant part of the global carbon budget. However, almost all available data on [C] in altered peridotite come from seafloor samples.

We compiled data on [C] in altered mantle peridotite from seafloor and ophiolite samples (Dataset S3). After eliminating outliers—six samples with much higher [C] than the other 223 samples—these data yield an average of 681 ± 45 ppm carbon (1σ). This is consistent with studies of metamorphosed seafloor peridotites (3, 20–22). Fig. 1 illustrates the relationship of [C] versus $H_2O$ content in altered peridotites. In turn, we relate this to the volume proportion of serpentine because almost all $H_2O$ in these samples is in serpentine.

## Subduction of Carbon-Bearing Sediments: 13–23 Mt C/y

[C] in oceanic sediments was reviewed by Rea and Ruff (23), Plank and Langmuir (24), and Plank (25). These studies do not fully account for organic carbon, particularly in pelagic sediments and turbidites. Where measured (e.g., ref. 26), organic carbon averages around 1 wt% in hemipelagic ooze that is nearly free of carbonate. Samples of such sediments in which [C] was not measured were assumed to be carbon free. On this basis, and the observation that these lithologies are more common than

### Significance

This paper reviews carbon fluxes into and out of subduction zones, using compiled data, calculations of carbon solubility in aqueous fluids, and estimates of carbon flux in metasedimentary diapirs. Upper-bound estimates suggest that most subducting carbon is transported into the mantle lithosphere and crust, whereas previous reviews suggested that about half is recycled into the convecting mantle. If upper-bound estimates are correct, and observed output from volcanoes and diffuse outgassing is smaller, then the mantle lithosphere is an important reservoir for carbon. If the subduction carbon cycle remains in balance, then outgassing from ridges and ocean islands is not balanced, so that the carbon content of the lithosphere + ocean + atmosphere has increased over Earth history.

Author contributions: P.B.K. and C.E.M. designed research, performed research, contributed new reagents/analytic tools, analyzed data, and wrote the paper.

Reviewers: J.J.A., Yale University; J.C., ETH Zurich; R.D., Rice University; and D.S., Johns Hopkins University.

The authors declare no conflict of interest.

Freely available online through the PNAS open access option.

[1]To whom correspondence may be addressed. Email: peterk@ldeo.columbia.edu or manning@epss.ucla.edu.

This article contains supporting information online at www.pnas.org/lookup/suppl/doi:10.1073/pnas.1507889112/-/DCSupplemental.

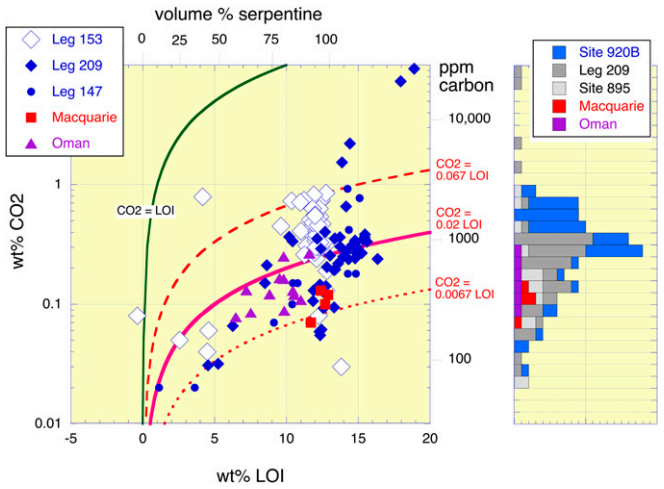


**Fig. 1.** Relationship of loss-on-ignition (LOI) to [$CO_2$] (left axis) and [C] (right axis) in altered mantle peridotites from ophiolites and midocean ridges. Top scale translates LOI to volume percent serpentine, assuming LOI is mainly $H_2O$ in serpentine with a density of 2,485 kg/m$^3$, and prealteration density is 3,300 kg/m$^3$. Contours show linear relationships between LOI and [$CO_2$], with intercept = 0 and slopes given on the left axis in red. Data sources in Dataset S3.

carbonates in subducting sediments (25), we retain the lower-bound flux of 13 Mt C/y in subducting sediments (1), but revise the upper bound from 17 Mt C/y to 23 Mt C/y (also see ref. 27).

Our analysis focuses on steady-state fluxes of carbon subducting to depths of ∼300 km on time scales of ∼10 Ma. Changing subduction rates, sedimentation rates, bottom water temperature, and changing oxidation states in the atmosphere and oceans, could have led to considerable variability in the nature and flux of subducting sedimentary carbon during Earth history (e.g., ref. 6). A relatively recent, significant factor was the mid-Mesozoic shift from formation of shelf carbonates to deposition of pelagic carbonates in the deep ocean (e.g., refs. 28–30). This may have changed the nature of carbon subduction, from periodic fluxes during continental collisions to a closer approach to steady state. Fluxes of subducting carbon also varied due to changes in the length and convergence rate of subduction zones worldwide (e.g., ref. 31). As with the possible temporal variability of [C] in oceanic crust, this is an important topic for future, comprehensive study.

## Carbon Uptake at the Outer Rise: 4–15 Mt C/y

The outer rise is a trench-parallel, bathymetric high caused by bending and faulting of oceanic plates before subduction (32, 33). Seismic studies show that active faults extend into the mantle at and near the outer rise, associated with serpentinization (*SI Text*). At the outer rise adjacent to the Central American subduction zone, a layer of mantle peridotite ∼10 km thick undergoes ∼10–30% serpentinization (13). Uncertainty in the proportion of serpentinization arises mainly from systematic along-strike variation in the nature of the subducting oceanic plate, as also seen for the Alaska subduction zone by Shillington et al. (34).

A preliminary assessment of carbon uptake can be made by assuming that [C] in serpentinized peridotites at the outer rise is similar to that of seafloor peridotites. Thus, for example, we infer that [C] in the upper 10 km of the mantle section of a subducting oceanic plate with 10% serpentine is 10% × 681 ± 45 ppm. These assumptions imply that outer-rise alteration takes up 4–15 Mt C/y. Our estimates are similar to those of Dasgupta (ref. 2; 1–10 Mt C/y) and Alt et al. (ref. 3; 0.16–1.9 Mt C/y) and, although clearly preliminary, show that mantle alteration at the outer rise may be significant in the global carbon cycle.

## Carbon Transfer into the Leading Edge of the Mantle Wedge (<300 °C and <1 GPa): 0.1–1.3 Mt C/y

Prior studies inferred that there is no significant transfer of carbon from the footwall into the hanging wall at subduction zone depths less than 60–70 km (e.g., refs. 1, 8, and 35). However, the presence of fully carbonated peridotites composed of magnesite + quartz and dolomite + quartz ("listvenites") in ophiolites thrust over metasediments suggests substantial carbon transfer at low temperatures ($T$) (36). For ∼15–20 million years starting at ∼96 Ma, the Samail ophiolite of Oman was thrust over oceanic crust and sediments (37, 38). Listvenites formed at ∼100 °C in partially serpentinized peridotite within 500 m of exposed contacts with footwall rocks. Their Rb/Sr age of 97 ± 17 Ma indicates formation during ophiolite emplacement. The thickest mapped layer contains ∼1 billion tons of $CO_2$. Samail listvenites have higher $^{87}Sr/^{86}Sr$ than Cretaceous to modern seawater, implying that Sr was derived from underlying sediments containing radiogenic $^{87}Sr/^{86}Sr$, and we infer that sediment-derived fluid was also the source of the $CO_2$ and Ca in the listvenites (36). At ∼100 °C along a shallow subduction zone geotherm of 5–15 °C/km, listvenite formation occurred at 7–20 km (0.2–0.6 GPa) based on thermal models of subduction zones (e.g., refs. 39 and 40), consistent with the thickness of the Samail ophiolite (5–7 km oceanic crust + up to 15 km of mantle peridotite).

Similar listvenites, some formed at higher $T$, are found elsewhere at and near the contact where peridotites are thrust over metasediments (*SI Text*). If such layers form above 1–10% of subduction zones worldwide, with an average thickness of 10–100 m, this corresponds to transfer of 0.06–6 Mt C/y into the leading edge of the mantle wedge. These values are highly uncertain, but we prefer intermediate values based on thermodynamic constraints on carbon flux out of subducting sediments in this depth interval (last paragraph of this section).

Seismic studies of subduction zones (*SI Text*) generally report a large proportion of serpentine in the leading edge of the mantle wedge, extending from the crust–mantle boundary to the arc–forearc transition (where heat flow abruptly increases away from the trench). Dataset S4 provides a compilation of estimates for the proportion of serpentine in these regions, and for the volume and mass of the serpentinized part of the wedge.

Intraoceanic subduction zones have thinner crust and more peridotite in the leading edge of the overthrust plate. Hydration of this peridotite at low $T$ forms chrysotile + lizardite serpentine polytypes (40). At greater depths, the higher-$T$ serpentine polytype, antigorite, is stable. Formation of antigorite may be geochemically very different from low-$T$ alteration of peridotite near the seafloor. Thus, our data on [C] in seafloor and ophiolite peridotite samples (*Carbon Uptake During Hydrothermal Alteration*) may have little bearing on [C] in antigorite peridotites. Nevertheless, there are no other data on [C] in this potentially important reservoir. In any case, the regions where antigorite could be stable comprise less than 33% of the forearc mantle, worldwide. Based on the data in Datasets S3 and S4, we estimate carbon flux associated with serpentinization in the leading edge of the mantle wedge to be 0.2–1.3 Mt C/y.

Thermodynamic calculations yield carbon solubilities of 50–500 ppm in aqueous fluids saturated in carbonate-bearing mudstone compositions in the pressure–temperature ($PT$) range for Oman listvenites (36). A combination of compaction (e.g., ref. 41) and clay dehydration (e.g., ref. 42) could produce ∼14–44 wt% aqueous fluid from carbonate-bearing, clay-rich sediments in this depth interval, yielding an upper bound of ∼1 Mt C/y. Larger fluxes of carbon could result from focusing of aqueous fluids from deeper metamorphic dehydration reactions.

## Carbon Transfer in Greenschist and Blueschist Facies (∼300–550 °C, 0.5–2 GPa): 0.001–0.6 Mt C/y

We were unable to find [C] data for metaperidotites believed to represent the "cold nose" of the mantle wedge. Many metaperidotites recording subduction zone metamorphism are inferred to represent subducted, seafloor peridotites that were serpentinized near slow-spreading midocean ridges. This is the case for

most or all such samples analyzed for bulk [C] (3, 21, 22). If these interpretations are correct, then [C] in these samples predates subduction, and provides little information on transfer of carbon from the footwall into the mantle wedge. Although they do not report [C], several other studies describe carbonate minerals, hydrocarbon-bearing fluid inclusions and/or graphite, in hanging-wall peridotites (*SI Text*). Carbon-bearing phases are also reported in talc and/or chlorite schists inferred to represent hanging-wall peridotites modified by mechanical mixing and chemical reaction metasediment and metabasalt (*SI Text*).

Studies of blueschist facies mélanges on Santa Catalina Island, CA, provide particularly comprehensive data (e.g., ref. 43 and references therein). Graphite and/or carbonate minerals are common in the matrix of blueschist and greenschist facies metasediments, and locally present in lawsonite–albite, blueschist and greenschist facies metasediments, and mafic rocks (44). They are major phases in hybridized metaperidotites and cross-cutting veins in 9 of 14 samples from lawsonite–albite facies, 3 of 18 samples from blueschist facies, and 2 of 11 samples from greenschist facies, and are minor phases in 9 other samples (45).

Our reconnaissance sampling at Santa Catalina revealed extensive zones of talc–carbonate rocks composed of calcite + dolomite + talc near the Pacific coast (Fig. 2). Our preliminary observations suggest that talc–carbonate rocks comprise 5–10% of the rock volume in this area. We hypothesize that they were not previously reported because they weather readily, and rarely form rocky outcrops. Talc–carbonate rocks, like listvenites, form via extensive reaction of $CO_2$-bearing aqueous fluids with mantle peridotite (e.g., refs. 46 and 47). In Oman and in several Canadian localities, talc–carbonate lithologies formed at ~250–300 °C (*SI Text*).

Ague and Nicolescu (48) recently highlighted the importance of $CaCO_3$ dissolution by aqueous fluids associated with blueschist facies metamorphism. We can make quantitative estimates of carbon solubility in aqueous fluids under these conditions using new data on the solubility of $CaCO_3$ minerals in aqueous fluids as a function of *P*, *T*, and salinity (reviews in refs. 11 and 12). We use data from Sverjensky et al. (49) and Facq et al. (50) for aqueous species to compute the solubility of stable $CaCO_3$ polymorphs as a function of *P* and *T* (Fig. 3). The solubility of $CaCO_3$ in pure $H_2O$, and in $H_2O$ saturated with model sediment (K-feldspar + muscovite ± quartz) and model peridotite (forsterite + enstatite) are nearly identical because the dominant aqueous electrolytes contributed by the silicate assemblages ($K^+$, $Mg^{+2}$, $MgOH^+$) are present in low concentrations relative to solutes from $CaCO_3$ dissolution.

**Fig. 2.** Examples of carbon-bearing rocks formed in subduction zones. (*Top Left*) Listvenites about 500 m above the basal thrust of the Samail ophiolite in Oman (36). (*Top Right*) Talc–carbonate rock near Little Harbor, Santa Catalina, CA. (*Bottom Left*) Marble in eclogite facies metasediments underlying the Higashi-Akaishi mantle peridotite, Japan. (*Bottom Right*) Magnesite-bearing dunite vein cutting chromitite band in in the Higashi-Akaishi peridotite.

Fig 3*A* shows that carbon solubility in fluids equilibrated with $CaCO_3$-bearing assemblages at ~300–550 °C and 0.5–2 GPa ranges from ~10 ppm to 2,000 ppm. If metamorphic reactions in this *PT* range generate 1–4 wt% aqueous fluid, this corresponds to global fluxes of 0.001–0.6 Mt C/y. These are probably minimum values. $CaCO_3$ solubility increases at a given *P* and *T* with decreasing pH associated with abundant charged aqueous clusters (e.g., ref. 12), with addition of NaCl (51), and decreasing $fO_2$ (52), which are all likely in subduction zones.

Cook-Kollars et al. (53) studied carbon mass transfer in blueschist facies metasediments in the Italian Alps. They found limited evidence for large-scale carbon loss due to interaction with aqueous fluids derived from deeper in the subducting plate, consistent with the estimates above. A caveat is that such studies potentially involve a sampling bias because it is difficult to identify former carbonate-bearing metasediments from which the original carbonate minerals have been entirely or extensively removed by dissolution.

## Carbon Transfer at High-Grade, Subsolidus Conditions (~550–800 °C, 2–6 GPa): 4–58 Mt C/y

As for lower-grade rocks described in the previous section, data on [C] in identified, mantle wedge peridotites in eclogite and ultra-high pressure (UHP) metamorphic facies are rare or absent. However, the presence of carbonate minerals, graphite, diamond and/or carbon-rich fluid inclusions is increasingly being noted in mantle wedge peridotites formed at eclogite and UHP facies (*SI Text*). Carbon-bearing phases are typically associated with amphibole- and/or phlogopite-bearing mineral assemblages, with hydration and carbonation attributed to input from subduction zones. Most identified mantle wedge localities were emplaced in continental collision zones rather than typical intraoceanic subduction zones. Although they provide information on carbon transfer, they do not yield direct constraints on fluxes during subduction of oceanic crust.

A notable exception is the Sanbagawa metamorphic belt, particularly in and around the Higashi-Akaishi garnet peridotite body, which overlies and was metamorphosed along with eclogite facies metasediments derived from the subducting Pacific plate (refs. 54 and 55 and *SI Text*). Olivine in the peridotites contains carbonate mineral inclusions and carbon-rich fluid inclusions (56–58). The Sanbagawa metasediments are less dense than peridotite at the same *PT* conditions. This buoyancy contrast is thought to have driven ascent of the lithologic package—including small bodies of peridotite—after high-*P* metamorphism (59). The metasediments include marbles that could have provided a source of dissolved carbon in aqueous fluids. On a recent trip to this area, we found that the peridotites include olivine–carbonate veins (Fig. 2), although the *PT* and timing of vein formation are not known.

Calculated carbon solubility in fluids equilibrated with metasediment at eclogite and UHP conditions could range from 0.1 to 3 wt% or more (Fig. 3). This is also the case for fluid equilibrated with metabasalt and serpentinite. Such high solubilities are consistent with [C] in fluid inclusions in diamond-bearing UHP metasediments (60). Dehydration of metasediments and metabasalts in this *PT* range could yield a few weight percent of fluid. Extraction of 1 wt% fluid corresponds to a global flux of 0.1–2.2 Mt C/y.

In addition, dehydration of serpentinites in the subducting mantle lithosphere supplies aqueous fluid that fluxes the overlying lavas and sediments (e.g., refs. 8, 61, and 62). The solubility of carbon in carbonate-saturated fluids derived from antigorite breakdown in peridotite is ~5,000 ppm (Fig. 3). On average, fully serpentinized peridotites have ~680 ppm carbon and ~14 wt% $H_2O$ in serpentine (*Carbon Uptake During Hydrothermal Alteration*). Thus, there is sufficient $H_2O$ to dissolve all of the carbonate minerals in the shallow mantle ($0.14 \times 5{,}000 = 700$ ppm).

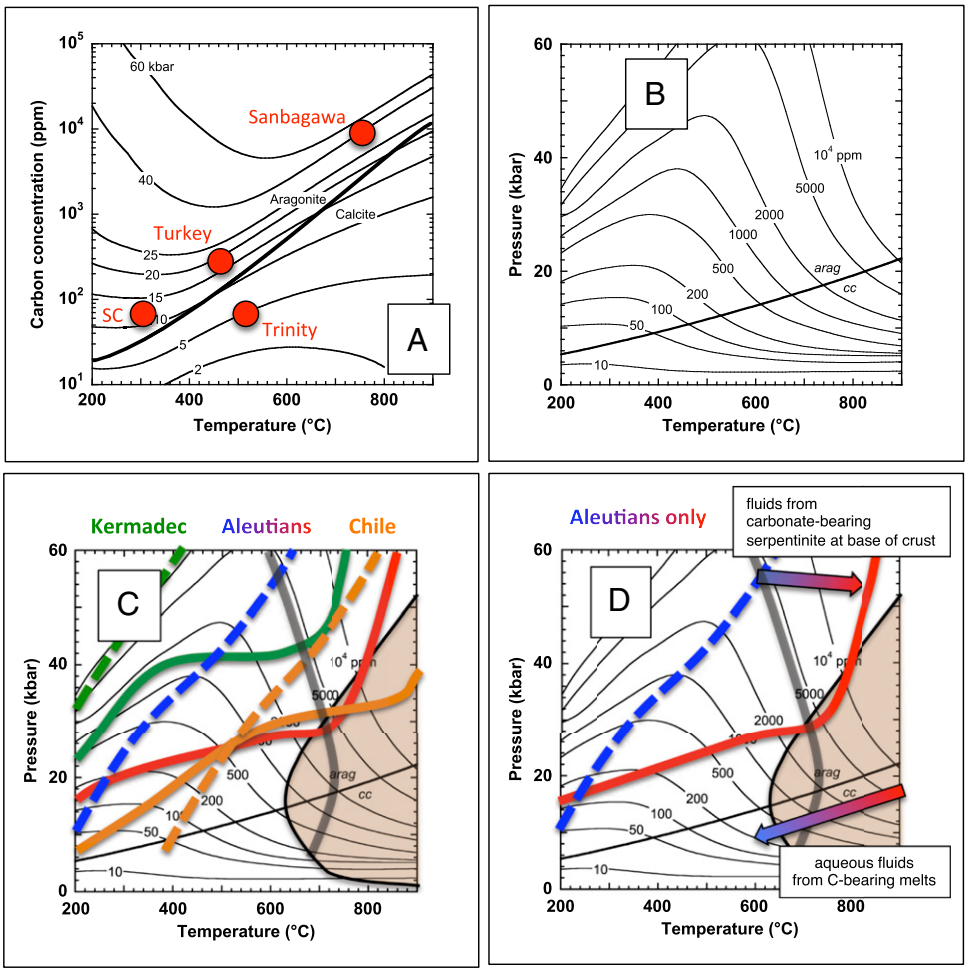


**Fig. 3.** Solubility of $CaCO_3$ in aqueous fluids (see *SI Text* for calculation methods and references). (*A*) Isobars of $CaCO_3$ solubility as a function of *T*. Red circles indicate *PT* solubility conditions for Santa Catalina; the basal thrust of the Trinity peridotite; lawsonite blueschists; and eclogite to UHP metamorphic terrains such as western Norway and the Higashi-Akaishi peridotite, Japan. (*B*) Contours of [C] in parts per million for aqueous fluids saturated in $CaCO_3$ as a function of *P* and *T*. (*C*) *B* overlain by 25× subduction zone geotherms of Syracuse et al. (39). Dashed lines, base of subducting oceanic crust; solid lines, top of subducting volcanics and sediments; green, Kermadec; blue and red, Aleutians; orange, southern Chile. Solid gray curve indicates stability limit of serpentine (118). Orange field indicates *PT* conditions above the fluid-saturated solidus for metabasalt and metasediment (69). (*D*) *B* with Aleutian geotherms. Upper arrow, *PT* trajectory for fluids produced by serpentine dehydration; lower arrow, *PT* trajectory for fluids rising into the mantle lithosphere and crust.

These fluids heat as they rise through the subducting plate, so carbon solubility will increase to several weight percent (Fig. 3). Even if they are close to carbonate saturation when generated, they can dissolve several weight percent carbon when they reach the top of the subducting plate. Reaction of carbonate-bearing metasediments and metabasalts with 10 wt% aqueous fluid derived from serpentinite dehydration could yield a global flux as high as 22 Mt C/y, provided that sufficient carbonate was present within the metasediments.

Carbonate dissolution in such fluids represents an additional carbon flux that must be added to the flux derived from models that do not account for mineral dissolution (8, 35, 63, 64). Their only source of carbon is the forward progress of decarbonation reactions (e.g., aragonite + quartz = wollastonite + $CO_2$); all minerals are assumed to be perfectly insoluble. However, Fig. 3 demonstrates that carbonate mineral solubility is actually quite high in $H_2O$-rich fluid at subuction zone conditions.

The open system calculations of Gorman et al. (8) afford the best estimate of carbon flux derived solely from decarbonation reactions in the absence of mineral dissolution. Their distillation model yields a global flux of about 4 Mt C/y from the subducting plate into the mantle wedge and provides a lower bound for carbon flux from the subducting plate in eclogite and UHP metamorphic facies. Their fluxed model, in which $H_2O$-rich serpentinite-derived fluid drives decarbonation reactions, yields a global flux of ~37 Mt C/y. We add the upper-bound dissolution and metamorphic fluxes of 22 Mt C/y to yield an upper bound of ~59 Mt C/y from the subducting plate in eclogite and UHP facies.

Mineral solubilities in $H_2O$ are lowered by addition of $CO_2$ derived from decarbonation reactions. However, the combination of low $CO_2$ mole fractions of subduction zone fluids [<0.2 (8)] and the relatively minor effect on $H_2O$ dielectric constant (65) will conspire to maintain high carbonate mineral solubilities, even in rocks undergoing decarbonation reactions.

These considerations have four important consequences for carbon mass transfer in subduction zones.

*i*) Fluid derived from serpentinite dehydration at eclogite-facies conditions can dissolve all of the carbonate formed in the shallow mantle before subduction.

*ii*) Fluid derived from serpentinites can dissolve much of the carbonate in subducting basalts and sediments (below the aqueous fluid-saturated solidus), and drive metamorphic decarbonation reactions, potentially removing all carbon from the subducting plate.

*iii*) Lithologic contrasts are unlikely to cause significant $CaCO_3$ precipitation due to the $CaCO_3$ solubility in pure $H_2O$, model metasediment, and model peridotite. The main controls on subsolidus $CaCO_3$ mobility are the *PT* gradient along the fluid flow path, and changes in salinity or $fO_2$.

*iv*) If they do not cause partial melting, carbon-bearing aqueous fluids that rise within the mantle will remain undersaturated with $CaCO_3$ as they heat within the hot corner of the wedge [high dT/dP (e.g., refs. 39 and 40)]. At shallower levels, decompression and cooling of rising fluids in the lithosphere will cause gradual precipitation of carbonate over a range of depths. Carbonate precipitation will occur mainly in serpentine-free peridotites at >600 °C, assuming local equilibrium.

### Carbon Transfer in Hydrous Melts Near the Aqueous Fluid-Saturated Solidus: Continues Mass Transfer from Aqueous Fluids

The $H_2O$-saturated solidus for metasediments and metabasalts extends almost linearly from ~625 °C at 2 GPa to ~925 °C at the second critical endpoint near 5.5 GPa (Fig. 3*C* and *SI Text*). When there is appreciable dissolved $CO_2$, the solidus shifts to higher *T* (~800 °C at 3 GPa to 925 °C at 5 GPa).

Thermal models indicate that the tops of some subducting plates attain temperatures above the fluid-saturated solidus, whereas others do not. There is a steep thermal gradient in the top of the subducting plate so that in all but the hottest subduction zones, most of the subducting plate is below the aqueous fluid-saturated solidus at 2–6 GPa (Fig. 3). In subduction zones in which fluid-saturated anatexis occurs, the fluid—which at any given time is unlikely to comprise more than 1 wt% of a given rock system—will dissolve in near-solidus, hydrous silicate melt. Near the solidus, this will produce a small degree melt with ~30 wt% $H_2O$ (66, 67). Dissolved $CO_2$ in the fluid will thus be diluted by ~33% in the melt compared with the fluid. Dissolution of carbonate-saturated fluid with ~3 wt% carbon (~11 wt% $CO_2$) would yield about 4 wt% $CO_2$ in the melt, less than or equal to solubility of $CO_2$ in silica-rich melts at ≥ 3 GPa (68). The solubility of $CO_2$ in melt and aqueous fluid becomes continuous at the second critical endpoint [~925 °C, 5.5 GPa (69)]. Above this *P* and *T*, $CO_2$ solubility in supercritical liquid is likely to be ~5 wt% or more.

With increasing *T* above the solidus, the melt fraction will rise, and [$CO_2$] will fall to values well below the concentration required for $CO_2$ saturation, allowing continued dissolution/melting of residual carbonate. Moreover, incremental delivery of small amounts of fluid, driving distillation of fluid-saturated partial melt, will gradually raise the time-integrated degree of melting and exhaust residual carbonate in most metasedimentary assemblages (68), except for carbonate-rich lithologies such as marbles.

### Carbon Transfer via Fluid-Absent Melting: Important only in the Hottest Subduction Zones

Above 800–1,050 °C at 2–5 GPa, remaining carbonate- and hydrous silicate-bearing, subducting lithologies (*SI Text*) will undergo fluid-undersaturated partial melting. Liquids will be silicate melt compositions, potentially rich in $CO_2$, that will rise farther into the mantle wedge where they will cause additional flux melting of peridotite (refs. 70, 71, and 72 and references therein). Once these compositions heat beyond, e.g., 900–1,050 °C at 3 GPa (figure 8 in ref. 70), no residual solid carbonates are likely to remain. However, such high *T*/*P* conditions are unlikely to be attained in all but the hottest subduction zones.

### Carbon Transfer via Buoyant Diapirs: Much of What's Left

Under $H_2O$-poor conditions, some metabasalt and metasediments will remain below their solidi along subduction geotherms well into the upper mantle (2). However, most metasediments are >200 kg/m$^3$ less dense than peridotite at subduction zone conditions. Kelemen et al. (73) and Behn et al. (14) predicted that, when they reach 700–900 °C at 75–250 km depth, slab top metasediment layers that are >100 m thick and ~200 kg/m$^3$ less dense than peridotite would form diapirs and rise into the mantle wedge. Marbles and carbonate-bearing metapelites are likely to be included in such diapirs (14, 74, 75). Hybrid subduction mélanges formed by mechanical mixing and chemical interaction are also likely to be buoyant, and to rise through the subduction channel or mantle wedge (76). Such mélanges can include substantial carbonate (*Carbon Transfer in Greenschist and Blueschist Facies*).

In subducting sedimentary sections worldwide, carbonate layer thicknesses commonly exceed 100 m, and carbon-bearing minerals are abundant within packages of low-density sediments whose average thickness is >500 m (25). Thus, most of the carbon remaining in subducting metasediments—up to 47 wt% of the total carbon in the subducting plate—is susceptible to transport through the mantle wedge in diapirs. Only thin metasedimentary layers and remaining, undissolved carbonate alteration in metabasalts and metaperidotites may pass this depth and be directly recycled into the convecting mantle.

The fate of metasedimentary diapirs within the mantle is speculative but important. The fluid-absent solidi for Ca and/or Mg carbonates are at more than 1,400–1,500 °C at mantle wedge pressures to ≥200 km depth, so the interiors of pure marble diapirs will remain solid (e.g., ref. 77). However, along the margins or rising diapirs, carbonate minerals + olivine + pyroxenes at *T* >1,250 °C will produce $CO_2$-rich melts (e.g., refs. 78 and 79).

Metasediments, including calc–silicates, that pass through the hot core of the mantle wedge will undergo high degrees of fluid-absent partial melting (*SI Text*). Certain xenoliths may represent the residue of such melting (80). The resulting melts will react with peridotite along the margins of partially molten diapirs. Where the melt–rock ratio is high and melts are hydrous, this could produce primitive andesites (81); at small melt–rock ratios and low $H_2O$ contents, the products are likely to be alkali basalts (70, 71). These melts will rise into the mantle lithosphere.

Thus, it is likely that almost all of the carbon in metasedimentary diapirs is transferred into carbonate-bearing silicate melts in the hot core of the mantle wedge. Melts from diapirs, plus slab-derived melts, plus fluid-fluxed melts of the mantle—and any remaining solid, marble cores—will rise into the mantle lithosphere and lower crust. Where they rise into the mantle at <1,250 °C, the melts will encounter the shelf in the carbonated peridotite solidus—extending from ~1,000 °C at 2 GPa to 1,250 °C at 1 GPa—where $CO_2$-rich fluid + olivine + pyroxene (+ garnet or spinel) become stable at low *P* with respect to $CO_2$-rich melt (Fig. 4). For melt with abundant dissolved $H_2O$ and $CO_2$, this will produce hydrous melts, some crystallization, and $CO_2$-rich fluid. For melts with little or no $H_2O$, this will cause extensive crystallization and produce abundant $CO_2$-rich fluid.

The solubility of carbon in aqueous fluids cooling from 900 °C to 600 °C and decompressing from 2 GPa to 1 GPa drops by a factor of ~100. Large amounts of carbonate would be precipitated from such rising fluids. Additional $CO_2$-rich fluid could emerge in volcanic arcs, contribute to diffuse emissions in regions flanking arc volcanoes, and/or form carbonate minerals in the lower crust (see next three sections). They could also form multicomponent brines that contribute to lower crustal granulite metamorphism (82–84).

In all of these scenarios, most of the $CO_2$ in metasedimentary diapirs would be transferred into the mantle lithosphere, arc crust, and/or ocean and atmosphere, instead of being transferred to the global, convecting mantle.

### Output from Arc Volcanoes: 18–43 Mt C/y

Reviews of gas fluxes from arc volcanoes (5, 63, 85) yield bounds on emissions from arc volcanoes from 18 Mt C/y to 43 Mt C/y, based on direct measurements of $SO_2$ concentration and flux in volcanic plumes, together with observed $CO_2/SO_2$ ratios in gases and fluids, and/or somewhat more indirect estimates of $^3$He flux, together with observed $^3He/CO_2$ ratios in gases, fluids, and volcanic glass. Direct measurements of $CO_2$ output from volcanoes are few. We expect that this will change soon, yielding better constraints. Burton et al. (5) emphasized that their estimate was

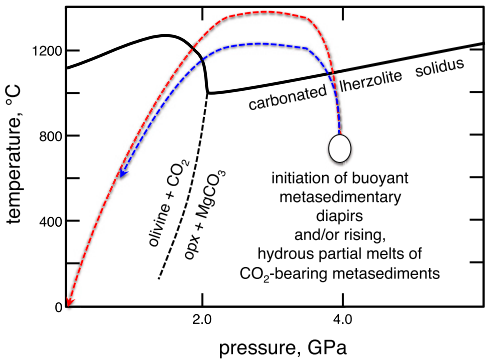


**Fig. 4.** *PT* trajectory for partial melts of subducting material and for buoyant diapirs. Melting of metabasalt and most metasediments, and melting along peridotite–marble contacts, will produce $CO_2$-bearing silicate melt. Reaction of these melts with peridotite will produce a range of $CO_2$+$H_2O$-bearing liquids from andesite to alkali basalt to carbonatite. $CO_2$-rich, $H_2O$-poor melts will crystallize and evolve $CO_2$-rich fluid at the carbonated lherzolite solidus (refs. 79 and 119 and additional references in *SI Text*). Hydrous melts will exsolve $CO_2$-rich fluids. Remaining melts and fluids will ascend past the carbonated lherzolite solidus and form carbon-bearing minerals in the mantle lithosphere and crust.

higher than that of Hilton et al. (85) and other recent reviews because of improving data quality and data density.

The source of $CO_2$ in arc volcano emissions can be ambiguous. Where $CO_2$ contents correlate with $^3$He, it is inferred that most of the $CO_2$ is introduced from the mantle into the base of arc crust. Where $CO_2$ and $^3$He are correlated, and $^3$He/$CO_2$ ratios are lower than in other tectonic settings, and/or where $\delta^{13}$C reflects input of nonmantle carbon, this is ascribed to recycling of carbon from subducting sediment and altered oceanic crust. However, arc volcanoes—particularly in continental arcs—may also emit $CO_2$ added to magmas during metamorphism of carbon-bearing lithologies within the crust (31).

$CO_2$ contents in melt inclusions in phenocrysts in arc lavas can be used to place lower bounds on $CO_2$ in parental magmas passing from the mantle into arc crust, as reviewed by Wallace (7). However, because the extent of prior degassing of $CO_2$ from decompressing melts currently cannot be determined with confidence, melt inclusion data have little utility in estimating an upper bound for magmatic input of $CO_2$ into arc lithosphere (e.g., ref. 86). Wallace (7) and Blundy et al. (86) arrive at similar estimates for $CO_2$ contents in primitive magmas passing from the mantle into arc crust. However, the estimate of Wallace was derived using inferred arc magma fluxes together with the volcanic $CO_2$ flux estimated by Hilton et al. (85), so these values are not independent. The estimate of Blundy et al. is based on the assumption that observed andesites are produced by 80% crystal fractionation from parental basalts, which could be too high; for example, using a value of 40% crystal fractionation would increase the estimated magmatic $CO_2$ flux by a factor of 2 compared with that of Hilton et al.

Additional studies of $^3$He/$CO_2$ are warranted to separate subduction zone versus arc crust contributions to $CO_2$ in arc volcanoes. Meanwhile, available results seem to indicate that most $CO_2$ emerging from arc volcanoes is derived from recycling of subducted $CO_2$. Estimates of $CO_2$ in parental magmas, before crystal fractionation, need to be refined.

### Diffuse Outgassing of Carbon at Forearcs and Arcs: 4–12 Mt C/y or More

Diffuse outgassing of subducted carbon as $CO_2$, methane, and other hydrocarbons could be an important part of the global carbon budget (5, 63, 87). However, even the most up-to-date reviews reflect measurements on a large range of scales that make it difficult to extract global estimates. We focus here on diffuse outgassing of $CO_2$ in arcs (forearc, arc, backarc). Evidence for such output is abundant. Haggerty and coworkers (ref. 88 and *SI Text*) first documented carbonate chimneys and authigenic carbonate deposited by fluids from subducting sediment and oceanic crust at and near seamounts in the Mariana and Bonin forearcs. Fryer and coworkers subsequently found

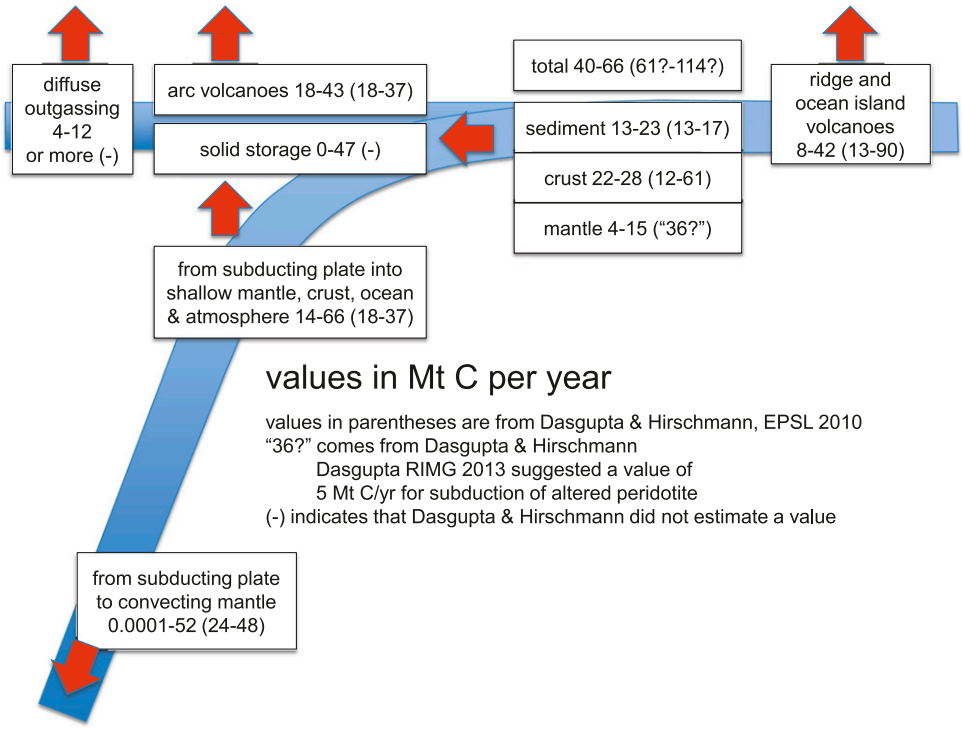


**Fig. 5.** Major fluxes of carbon estimated in this paper, with values from Dasgupta and Hirschmann (1) for comparison.

more examples in their studies of serpentine diapirs in the Mariana forearc (review in ref. 89).

Campbell et al. (90) list six other sites where active, diffuse outgassing of $CO_2$ and/or hydrocarbons has been detected in forearcs, and 10 more localities where evidence suggests that this happened in the past. In some cases, oxygen isotope data are indicative of derivation from a high-$T$ source (e.g., refs. 91–93). However, unlike the Mariana seamounts, it is not clear in most cases how much carbon is derived from continental margin sedimentation, and from sediments in an accretionary prism, versus from subducting sediment.

There is venting of dense $CO_2$ liquid at hydrothermal sites on the flanks of submarine, Okinawa backarc and Mariana arc volcanoes (94–96). Because the water column in the Mariana arc has high, correlated $CO_2/^3He$ ratios indicative of significant, diffuse outgassing, Resing et al. (97) suggest global $CO_2$ fluxes from submarine volcanoes (based on $CO_2/^3He$ ratios and global $^3He$ systematics) should be revised upward.

There are a few regional studies of diffuse $CO_2$ flux in arcs that can be used to make a global estimate. Both focus on magmatic $CO_2$ in spring water, in hot springs in the Taupo volcanic zone of New Zealand, and in both hot and cold springs in the Oregon Cascades. Seward and Kerrick (98) estimated a diffuse flux of 12 Mt C/y associated with Pacific Rim volcanism. For the central Oregon Cascades, James et al. (99) estimate a diffuse magmatic $CO_2$ degassing rate of $3.4 \times 10^5$ kg/y per kilometer of arc, or about 4 Mt C/y over the 44,454 km of global subduction zones. We suspect that these values are underestimates.

## Little Evidence for Storage in Arc Crust

In arc crustal sections, carbonate and calc–silicate veins formed at lower crustal and Moho depths have been observed, cross cutting arc plutonic rocks (100–105). These may provide important information on degassing from decompressing magmas, and/or from the complete crystallization of magmas at depth. However, such veins do not appear to be common.

Many intermediate to felsic plutonic rocks are liquids that underwent complete crystallization in arc middle crust (e.g., refs. 73, 106, and 107). If these magmas contained ~1.5 wt% $CO_2$ as inferred for intermediate arc magmas by Blundy et al. (86), their crystallization must have released substantial $CO_2$. Given the paucity of carbonate observed so far in oceanic arc middle and lower crust, this $CO_2$ must have been deposited within upper crustal sedimentary and volcanic rocks, or emitted via diffuse outgassing (*Diffuse Outgassing of Carbon*).

**Table 1. Summary of carbon flux estimates**

| | Mt C/y | |
|---|---|---|
| Tectonic setting | Min | Max |
| Total carbon input to subduction zones | 40 | 66 |
| Total outputs from subduction zones including fluid flux and solubility + metamorphic reactions + diapirs | 14 | 66 |
| Output to atmosphere at subaerial arc volcanoes | 18 | 43 |
| Diffuse output to ocean and atmosphere in arc systems | 4 | 12 or more? |
| Storage in shallow, conductively cooled mantle ("lithosphere") and crust | 0 | 47 |
| Subducted carbon into convecting mantle | 0.0001 | 52 |
| Output to ocean and atmosphere at ridges and ocean islands | 8 | 42 |

## Summary: A Likely Carbon Reservoir in the Mantle Lithosphere

Our average value of [C] in altered oceanic crust agrees with Alt and Teagle (15), but our compilation provides stronger constraints and clearer bounds on the uncertainty of this estimate. Similarly, [C] in samples of altered peridotites from the seafloor and ophiolites, together with seismic data on the depth and proportion of serpentinization at the outer rise, provides an improved constraint on [C] in subducting oceanic mantle. Consideration of organic carbon caused us to raise the upper bound for [C] in subducting sediments compared with Plank and coworkers (e.g., refs. 24 and 25). In sum, we estimate that subducting plates, including sediments, carry 39–66 Mt C/y into subduction zones.

Although listvenites formed by carbon mass transfer from subducting sediment into mantle peridotite at low $T$ (<300 °C) are striking, we find that this flux and that in blueschist facies only account for transfer of 0–4 Mt C/y. Because carbonate solubility increases roughly along subduction zone geotherms, low-$PT$ flux is much less important than carbon transport in eclogite facies at >550 °C.

Dissolution of carbonate from altered oceanic crust and sediments into migrating aqueous fluids in eclogite facies, combined with metamorphic decarbonation reactions, could transfer 4–59 Mt C/y into the hanging wall, for assumed bounds of 1–10 wt% fluid passing through the upper part of the subducting plate. In addition, metasedimentary layers more than ~100 m thick are likely to form buoyant diapirs, carrying much of the remaining sedimentary carbon into the mantle wedge at 700–900 °C. Melting of diapirs, subducting sediments and volcanics, and fluid-fluxed mantle peridotite will produce $CO_2$-bearing liquids that pass through the hot core of the mantle wedge and ascend into the overlying plate, precipitating carbonate minerals in mantle lithosphere and lower crust.

These considerations yield a total flux of 14–69 Mt C/y into arc lithosphere (forearc to backarc). Provided that fluid flow is diffusely distributed, dissolving most of the carbonate in altered oceanic crust, we expect that the correct flux is likely to be close to the maximum estimate, and that little carbon is recycled into the convecting mantle via subduction.

The upper bound is substantially higher than current estimates for combined volcanic and diffuse flux from arc systems into the ocean and atmosphere. Observed [C] in arc lower crust is small. If these values are correct, significant quantities of carbon are stored in the mantle lithosphere. Very large fluxes correspond to small [C], if carbon is distributed uniformly. For example, if arc mantle lithosphere is 20 km thick, extending from 50 km to 250 km from the trench, with an average age of 40 million years, then [C] of 1,000 ppm in this volume would correspond to precipitation of ~16 Mt C/y in the lithosphere. This is sufficient—together with output from arc volcanoes and diffuse venting—to balance the maximum estimated input of 69 Mt C/y into arc lithosphere. A campaign of geochemical analyses will be necessary to investigate the extent of a lithospheric mantle carbon reservoir. The residence time and long-term fate of carbon in such a reservoir is unclear. Much could remain in the continental upper mantle for billions of years, while some might return to the convecting mantle via delamination (108, 109).

## Global Mass Balance

Global fluxes of carbon from Earth's interior to the surface, via magmatism at midocean ridges, within plate settings and arcs, plus diffuse fluxes, are highly uncertain. Marty et al. (110) reviewed and updated $CO_2$ output due to midocean ridge magmatism to reach an estimate of 8–21 Mt C/y. Similarly, Resing et al. (111) estimate a ridge flux of 6–24 Mt C/y. Marty and Tolstikhin (112) emphasized that the flux due to within-plate volcanism is uncertain, but is probably 10–100% of the ridge flux. The resulting range of values for combined carbon output from ridge and within-plate volcanism (8–42 Mt C/y) is reflected in Fig. 5 and discussed in *SI Text*.

Most carbon is probably extracted from subducting plates via dissolution of carbonates in aqueous fluid, evolution of $CO_2$-rich fluid in metamorphic decarbonation reactions, and ascent in metasedimentary diapirs. In turn, most of this carbon will pass through the convecting mantle wedge and be returned to the mantle lithosphere, the crust, and—via volcanoes and diffuse outgassing—the oceans and the atmosphere. Thin metasedimentary layers, and some carbonate in altered oceanic crust, may continue to subduct into the deeper mantle, but this could involve a small fraction of total subducted carbon. Large changes in the influx of subducting carbon might lead to large changes in output. For example, if Cretaceous subduction zones were twice as long, and consumed thicker carbonate sediment sections (31), this probably produced more numerous and/or larger metasedimentary diapirs. Thus, temporal changes in subduction inputs and outputs are likely to be strongly correlated, whereas the rate of recycling of carbon into the convecting mantle may be nearly independent of the rate of input at subduction zones.

If the subduction zone carbon cycle is nearly balanced during subduction to 50–300 km depth (5–10 Ma), so that there is little recycling into the convecting mantle, and this has persisted over most of Earth history, then what about global fluxes of carbon out of the convecting mantle? Marty et al. (110) infer that most carbon output from midocean ridges and ocean islands is primordial carbon from "less-degassed" mantle reservoirs. If so, and if subduction zones return far less carbon to the convecting mantle than is extracted at ridges and ocean islands, then the proportion of carbon in the mantle lithosphere + crystalline crust + sediments + ocean + atmosphere must be increasing over time. Among these shallow reservoirs, carbon-bearing sediments and the mantle lithosphere are the most important.

Hayes and Waldbauer (27) reviewed [C] in continental crust, primarily in sediments. They estimated $10 \times 10^{10}$ Mt carbon in the crust, intermediate between estimates from Holser et al. (113) and Wilkinson and Walker (114). In addition, if the upper 50 km of the mantle lithosphere contains 100–1,000 ppm carbon, for a continental area of $2.1 \times 10^8$ km$^2$ (115), this corresponds to $\sim 0.35–3.5 \times 10^{10}$ Mt C. Taking these estimates at face value, the continents (crust + mantle) contain $9.2–14.7 \times 10^{10}$ Mt C. Hayes and Waldbauer favor a nearly constant rate of growth of the continental crust (figure 7 in ref. 27), starting at 3.8 Ga. Thus, the net flux of $CO_2$ from the convecting mantle into the continents is 24–39 Mt C/y. These values are comparable to the estimates we summarized above, for midocean ridge plus within-plate fluxes, of 8–42 Mt C/y. Thus, it is plausible that ridge plus within-plate carbon output has caused a steady increase in the carbon inventory of the plates + oceans + atmosphere throughout Earth history, with very little recycling of carbon into the convecting mantle.

Carbon isotopes imply that at least 30% of diamonds contain recycled, sedimentary carbon (e.g., ref. 116). This recycled carbon may have been derived from fluids and/or melts carrying carbon from subducting sediment at 50–300 km within ~10 Ma of subduction, via processes described in this paper. However, a subset of diamonds—including some with inferred, recycled carbon—contain transition zone and lower mantle minerals. This suggests that some sedimentary carbon is indeed recycled into the convecting mantle on long time scales.

It is instructive to use diamond occurrences to place a lower bound on the flux of recycled sedimentary carbon into the convecting mantle. For the sake of argument, suppose that all diamonds, regardless of their carbon isotopes and mineral inclusions, formed from sedimentary carbon recycled into the convecting mantle. Most diamond occurrences are in kimberlite pipes. The probability that a kimberlite will be an economic diamond deposit is ~0.5% (117). The median concentration of diamonds in economic kimblerlite deposits in 1992 was ~17 ppb. The average concentration in noneconomic kimberlites (less than 2 ppb in 1992, extending to zero) is negligible. Thus, taking the kimberlite data as representative of the whole mantle, the concentration of diamond is 83 ppt, yielding $3 \times 10^5$ Mt of "recycled" carbon, approximately 300 thousand times smaller than the carbon inventory of the crust. This corresponds to recycling of $\sim 10^{-4}$ Mt C/y into the convecting mantle over 3.8 Ga.

## Methods

Carbon concentrations in peridotite rock powders (Dataset S5) were measured with a Carbon Analyzer (LECO CS 844) with modules to determine total carbon (TC) and total inorganic carbon (TIC). For TC, samples in a ceramic boat were combusted in $O_2$ at ~ 1,000 °C. Evolved $CO_2$ in $O_2$ carrier gas was absorbed in a titration cell with ethanolamine and a colorimetric indicator. $CO_2$ concentration was determined via optical spectroscopy. For TIC, samples were titrated with perchloric acid and heated to 80 °C. Evolved $CO_2$ was measured as for TC. Samples previously analyzed by Schwarzenbach et al. (22) were analyzed to check accuracy and precision.

## Conclusions: What Goes Down, Mostly Comes Up

Table 1 and Fig. 5 summarize fluxes estimated in this paper. Our upper-bound estimates indicate that almost all of the carbon in subducting sediments and oceanic plates may be extracted in fluids and melts that rise into the mantle wedge, and then—in buoyant solid diapirs and/or dissolved in fluids and melts—into the overlying plate. In contrast, previous reviews suggested that about half of subducting carbon is carried into the global, convecting mantle as part of the subducting oceanic plate.

When the influx of subducting carbon is larger than at present, it seems likely that the outflux will grow proportionately, so that balance between input and output may be maintained. If (*i*) our upper-bound estimates for carbon output from subducting plates are close to the actual fluxes, (*ii*) this carbon is transported through the mantle wedge into the mantle lithosphere and crust, and (*iii*) observed carbon output from volcanoes plus diffuse outgassing is smaller, then the mantle lithosphere is an important reservoir for carbon. Some carbon stored in the mantle lithosphere may eventually be recycled into the convecting mantle via delamination, while another component may remain indefinitely within the cratonic upper mantle.

Finally, if the subduction zone carbon cycle is approximately in balance, and if this is maintained over geologically significant times, then outgassing from midocean ridges and within-plate volcanic centers is not balanced and represents a net flux from the mantle to Earth's surface. This possibility is broadly consistent with data on the carbon content of the continents, noble gas systematics, and constraints on the amount of recycled carbon incorporated in mantle diamonds.

Most of our estimates are highly uncertain. We lack quantitative data on [C] in key reservoirs. Additional data on the proportion and age of carbon-bearing minerals in eclogite facies and mantle wedge lithologies would be particularly valuable because this is the *PT* regime in which thermodynamic calculations yield the largest and most uncertain fluxes of carbon from the subducting plate into the mantle. We expect that data on [C] in high-grade metamorphic rocks and peridotites will become more abundant over the coming decade. Care will be needed to determine the timing and *PT* conditions during formation of carbon-bearing minerals in these settings because eclogites and wedge peridotites have surely been affected by other processes, before and after subduction zone metamorphism.

**ACKNOWLEDGMENTS.** We thank J. Ague, J. Connolly, R. Dasgupta, and D. Sverjensky for reviews; B. Hacker for joining a quixotic venture on Santa Catalina; M. Grove for spurring us on our way; the Two Tomos, Mizukami and Morishita, for hospitality in the Sanbagawa area; G. Bernasconi-Green for sharing data; T. Plank, R. Coggon, and D. Teagle for input on [C] in subducting materials; J. Alt and G. Harlow for sharing samples used as [C] standards; A. Hofmann, B. Marty, and M. Walter for advice on mantle carbon budgets; and H. Magunn, D. Vaccaro, and M. Stonor for carbon analyses. This research was supported by National Science Foundation Grants EAR-1049905 (to P.K.) and EAR-1347987 (to C.M.) and the Deep Carbon Observatory.

1. Dasgupta R, Hirschmann MM (2010) The deep carbon cycle and melting in Earth's interior. *Earth Planet Sci Lett* 298:1–13.

2. Dasgupta R (2013) Ingassing, storage, and outgassing of terrestrial carbon through geologic time. *Rev Mineral Geochem* 75:183–229.

3. Alt JC, et al. (2013) The role of serpentinites in cycling of carbon and sulfur: Seafloor serpentinization and subduction metamorphism. *Lithos* 178:40–54.
4. Jarrard RD (2004) Subduction fluxes of water, carbon dioxide, chlorine, and potassium. *Geochem Geophys Geosyst* 4(5):8905.
5. Burton MR, Sawyer GM, Granieri D (2013) Deep carbon emissions from volcanoes. *Rev Mineral Geochem* 75:323–354.
6. Johnston FKB, Turchyn AV, Edmonds M (2011) Decarbonation efficiency in subduction zones: Implications for warm Cretaceous climates. *Earth Planet Sci Lett* 303:143–152.
7. Wallace PJ (2005) Volatiles in subduction zone magmas: Concentrations and fluxes based on melt inclusion and volcanic gas data. *J Volcanol Geotherm Res* 140:217–240.
8. Gorman PJ, Kerrick DM, Connolly JAD (2006) Modeling open system metamorphic decarbonation of subducting slabs. *Geochem Geophys Geosyst* 7(4):Q04007.
9. Kelemen PB, et al. (2011) Rates and mechanisms of mineral carbonation in peridotite: Natural processes and recipes for enhanced, in situ $CO_2$ capture and storage. *Annu Rev Earth Planet Sci* 39:545–576.
10. Fruh-Green GL, Connolly JAD, Plas A (2004) Serpentinization of oceanic peridotites: Implications for geochemical cycles and biological activity. *The Subseafloor Biosphere at Mid-Ocean Ridges*, eds Wilcock WSD, et al. (Am Geophys Union, Washington, DC), pp 119–136.
11. Manning CE, Shock EL, Sverjensky DA (2013) The chemistry of carbon in aqueous fluids at crustal and upper-mantle conditions: Experimental and theoretical constraints. *Rev Mineral Geochem* 75:109–148.
12. Manning CE (2013) Thermodynamic modeling of fluid-rock interaction at mid-crustal to upper mantle conditions. *Rev Mineral Geochem* 76:135–164.
13. Van Avendonk HJA, Holbrook WS, Lizarralde D, Denyer P (2011) Structure and serpentinization of the subducting Cocos plate offshore Nicaragua and Costa Rica. *Geochem Geophys Geosyst* 12(6):Q06009.
14. Behn MD, Kelemen PB, Hirth G, Hacker BR, Massonne HJ (2011) Diapirs as the source of the sediment signature in arc lavas. *Nat Geosci* 4:641–646.
15. Alt JC, Teagle DAH (1999) The uptake of carbon during alteration of oceanic crust. *Geochim Cosmochim Acta* 63:1527–1535.
16. Carlson RL (2001) The abundance of ultramafic rocks in the Atlantic Ocean crust. *Geophys J Int* 144:37–48.
17. Cannat M, et al. (1995) Thin crust, ultramafic exposure and rugged faulting patterns at the Mid-Atlantic Ridge (22°–24°N). *Geology* 23:49–52.
18. DeMets C, Gordon RG, Argus DF, Stein S (1990) Current plate motions. *Geophys J Int* 101:425–478.
19. Bird P (2003) An updated digital model of plate boundaries. *Geochem Geophys Geosyst* 4(3):1027.
20. Alt JC, et al. (2012) Uptake of carbon and sulfur during seafloor serpentinization and the effects of subduction metamorphism in Ligurian peridotites. *Chem Geol* 322-323:268–277.
21. Alt JC, et al. (2012) Recycling of water, carbon, and sulfur during subduction of serpentinites: A stable isotope study of Cerro del Almirez, Spain. *Earth Planet Sci Lett* 327-328:50–60.
22. Schwarzenbach EM, Fruh-Green GL, Bernasconi SM, Alt JC, Plas A (2013) Serpentinization and carbon sequestration: A study of two ancient peridotite-hosted hydrothermal systems. *Chem Geol* 351:115–133.
23. Rea DK, Ruff LJ (1996) Composition and mass flux of sediment entering the world' s subduction zones: Implications for global sediment budgets, great earthquakes, and volcanism. *Earth Planet Sci Lett* 140:1–12.
24. Plank T, Langmuir CH (1998) The chemical composition of subducting sediment and its consequences for the crust and mantle. *Chem Geol* 145:325–394.
25. Plank T (2014) The chemical composition of subducting sediments. *The Crust*, Treatise on Geochemistry, ed Rudnick RL (Elsevier-Pergamon, Oxford), 2nd Ed, Vol 4, pp 607–629.
26. Mayer L, Pisias N, Janacek T (1992) *Proceedings of the Ocean Drilling Program, Initial Reports* (Ocean Drill Program, College Station, TX), Vol 138.
27. Hayes JM, Waldbauer JR (2006) The carbon cycle and associated redox processes through time. *Philos Trans R Soc Lond B Biol Sci* 361(1470):931–950.
28. Ridgwell A (2005) A mid Mesozoic revolution in the regulation of ocean chemistry. *Mar Geol* 217:339–357.
29. Falkowski PG, et al. (2004) The evolution of modern eukaryotic phytoplankton. *Science* 305(5682):354–360.
30. Winterer EL (2001) The oldest biogenous pelagic sediments above Mesozoic oceanic basement: A review. *Paradoxes in Geology*, eds Briegel U, Xiao W (Elsevier, Amsterdam), pp 373–385.
31. Lee C-TA, et al. (2013) Continental arc–island arc fluctuations, growth of crustal carbonates, and long-term climate change. *Geosphere* 9:21–36.
32. Caldwell JG, Haxby WF, Karig DE, Turcotte DL (1976) Applicability of a universal elastic trench profile. *Earth Planet Sci Lett* 31:239–246.
33. Chapple WM, Forsyth DW (1979) Earthquakes and bending of plates at trenches. *J Geophys Res* 84:6729–6749.
34. Shillington DJ, et al. (2014) Controls on abrupt changes in faulting, hydration and seismicity in the Alaska subduction zone. *Nature*, in press.
35. Kerrick DM, Connolly JAD (2001) Metamorphic devolatilization of subducted oceanic metabasalts: Implications for seismicity, arc magmatism and volatile recycling. *Earth Planet Sci Lett* 189:19–29.
36. Falk ES, Kelemen PB (2015) Geochemistry and petrology of listvenite in the Somali ophiolite, Sultanate of Oman: Complete carbonation of peridotite during ophiolite emplacement. *Geochim Cosmochim Acta* 160:70–90.
37. Boudier F, et al. (1985) Kinematics of oceanic thrusting in the Oman ophiolite: Model of plate convergence. *Earth Planet Sci Lett* 75:215–222.
38. Hacker BR, Gnos E (1997) The conundrum of Samail: Explaining the metamorphic history. *Tectonophys.* 279:215–226.
39. Syracuse EM, van Keken PE, Abers GA (2010) The global range of subduction zone thermal models. *Phys Earth Planet Inter* 183:73–90.
40. Wada I, Wang K (2009) Common depth of slab-mantle decoupling: Reconciling diversity and uniformity of subduction zones. *Geochem Geophys Geosyst* 10(10): Q10009.
41. Bond GC, Kominz MA (1984) Construction of tectonic subsidence curves for the early Paleozoic miogeocline, southern Canadian Rocky Mountains: Implications for subsidence mechanisms, age of breakup, and crustal thinning. *Geol Soc Am Bull* 95:155–173.
42. Lynch FL (1997) Frio shale mineralogy and the stoichometry of the smectite-to-illite reaction: The most important reaction in clastic sedimentary diagenesis. *Clays Clay Miner* 45:618–631.
43. Grove M, et al. (2008) The Catalina Schist: Evidence for middle Cretaceous subduction erosion of southwestern North America. *Spec Pap Geol Soc Am* 436:335–361.
44. Bebout GE, Barton MD (1989) Fluid flow and metasomatism in a subduction zone hydrothermal system: Catalina Schist terrane. *Calif Geol* 17:976–980.
45. Bebout GE, Barton MD (1993) Metasomatism during subduction: Products and possible paths in the Catalina Schist, California. *Chem Geol* 108:61–92.
46. Naldrett AJ (1966) Talc-carbonate alteration of some serpentinized ultramafic rocks south of Timmins, Ontario. *J Petrol* 7:489–499.
47. Schandl ES, Naldrett AJ (1992) $CO_2$ metasomatism of serpentinites south of Timmins, Ontario. *Can Mineral* 30:93–108.
48. Ague JJ, Nicolescu S (2014) Carbon dioxide released from subduction zones by fluid-mediated reactions. *Nat Geosci* 7:355–360.
49. Sverjensky DA, Harrison B, Azzolini D (2014) Water in the deep Earth: The dielectric constant and the solubilities of quartz and corundum to 60kb and 1200° C. *Geochim Cosmochim Acta* 129:125–145.
50. Facq S, Daniel I, Montagnac G, Cardon H, Sverjensky DA (2014) In situ Raman study and thermodynamic model of aqueous carbonate speciation in equilibrium with aragonite under subduction zone conditions. *Geochim Cosmochim Acta* 132:375–390.
51. Newton RC, Manning CE (2002) Experimental determination of calcite solubility in $H_2O$-NaCl solutions at deep crust/upper mantle pressures and temperatures: Implications for metasomatic processes in shear zones. *Am Mineral* 87:1401–1409.
52. Lazar C, Young ED, Manning CE (2012) Experimental determination of equilibrium nickel isotope fractionation between metal and silicate from 500 °C to 950 °C. *Geochim Cosmochim Acta* 86:276–295.
53. Cook-Kollars J, Bebout GE, Collins NC, Angiboust S, Agard P (2014) Subduction zone metamorphic pathway for deep carbon cycling: I. Evidence from HP/UHP metasedimentary rocks, Italian Alps. *Chem Geol* 386:31–48.
54. Aoya M, Endo S, Mizukami T, Wallis SR (2013) Paleo-mantle wedge preserved in the Sambagawa high-pressure metamorphic belt and the thickness of forearc continental crust. *Geology* 41:451–454.
55. Endo S, Tsuboi M (2013) Petrogenesis and implications of jadeite-bearing kyanite eclogite from the Sanbagawa belt (SW Japan). *J Metamorph Geol* 31:647–661.
56. Enami M, Mizukami T, Yokoyama K (2004) Metamorphic evolution of garnet-bearing ultramafic rocks from the Gongen area, Sanbagawa belt, Japan. *J Metamorph Geol* 22:1–15.
57. Hirai H, Arai S (1987) $H_2O$-$CO_2$ fluids supplied in alpine-type mantle peridotites: Electron petrology of relic fluid inclusions in olivines. *Earth Planet Sci Lett* 85:311–318.
58. Arai S, Ishimaru S, Mizukami T (2012) Methane and propane micro-inclusions in olivine in titanoclinohumite bearing dunites from the Sanbagawa high-P metamorphic belt, Japan: Hydrocarbon activity in a subduction zone and Ti mobility. *Earth Planet Sci Lett* 353-354:1–11.
59. Aoki K, et al. (2009) Metamorphic P–T–time history of the Sanbagawa belt in central Shikoku, Japan and implications for retrograde metamorphism during exhumation. *Lithos* 113:393–407.
60. Frezzotti ML, Selverstone J, Sharp ZD, Compagnoni R (2011) Carbonate dissolution during subduction revealed by diamond-bearing rocks from the Alps. *Nat Geosci* 4: 703–706.
61. Hacker BR (2008) $H_2O$ subduction beyond arcs. *Geochem Geophys Geosyst* 9(3): Q03001.
62. van Keken PE, Hacker BR, Syracuse EM, Abers GA (2011) Subduction factory: 4. Depth-dependent flux of $H_2O$ from subducting slabs worldwide. *J Geophys Res* 116(B1):B01401.
63. Kerrick DM (2001) Present and past nonanthropogenic $CO_2$ degassing from the solid earth. *Rev Geophys* 39:565–585.
64. Kerrick DM, Connolly JAD (1998) Subduction of ophicarbonates and recycling of $CO_2$ and $H_2O$. *Geology* 26(4):375–378.
65. Galvez ME, Manning CE, Connolly JAD, Rumble D (2015) The solubility of rocks in metamorphic fluids: Theory and example of graphite-bearing pelite to 900 °C and 3 GPa. *Earth Planet Sci Lett*, in press.
66. Mysen BO, Wheeler K (2000) Solubility behavior of water in haploandesitic melts at high pressure and high temperature. *Am Mineral* 85:1128–1142.
67. Kawamoto T, Holloway JR (1997) Melting temperature and partial melt chemistry of $H_2O$-saturated mantle peridotite to 11 Gigapascals. *Science* 276(5310):240–243.
68. Duncan MS, Dasgupta R (2014) $CO_2$ solubility and speciation in rhyolitic sediment partial melts at 1.5–3.0 GPa – Implications for carbon flux in subduction zones. *Geochim Cosmochim Acta* 124:328–347.
69. Schmidt MW, Vielzeuf D, Auzanneau E (2004) Melting and dissolution of subducting crust at high pressures: The key role of white mica. *Earth Planet Sci Lett* 228:65–84.
70. Mallik A, Dasgupta R (2013) Reactive infiltration of MORB-eclogite-derived carbonated silicate melt into fertile peridotite at 3 GPa and genesis of alkalic magmas. *J Petrol* 53:2267–2300.
71. Mallik A, Dasgupta R (2012) Reaction between MORB-eclogite derived melts and fertile peridotite and generation of ocean island basalts. *Earth Planet Sci Lett* 329-330:97–108.

72. Mallik A, Dasgupta R (2014) Effect of variable $CO_2$ on eclogite-derived andesite and lherzolite reaction at 3 GPa—Implications for mantle source characteristics of alkalic ocean island basalts. *Geochem Geophys Geosyst* 15:1533–1557.
73. Kelemen PB, Hanghøj K, Greene A (2003) One view of the geochemistry of subduction-related magmatic arcs, with an emphasis on primitive andesite and lower crust. *The Crust*, Treatise on Geochemistry, ed Rudnick RL (Elsevier-Pergamon, Oxford), Vol 3, pp 593–659.
74. Tsuno K, Dasgupta R, Danielson L, Righter K (2012) Flux of carbonate melt from deeply subducted pelitic sediments: Geophysical and geochemical implications for the source of Central American volcanic arc. *Geophys Res Lett* 39(16):L16307.
75. Tsuno K, Dasgupta R (2011) Melting phase relation of nominally anhydrous, carbonated pelitic-eclogite at 2.5–3.0 GPa and deep cycling of sedimentary carbon. *Contrib Mineral Petrol* 161:743–763.
76. Marschall HR, Schumacher JC (2012) Arc magmas sourced from mélange diapirs in subduction zones. *Nat Geosci* 5:862–867.
77. Wyllie PJ, Huang W-L (1976) Carbonation and melting reactions in the system CaO-MgO-$SiO_2$-$CO_2$ at mantle pressures with geophysical and petrological applications. *Contrib Mineral Petrol* 54:79–107.
78. Dasgupta R, Hirschmann MM, Smith ND (2007) Water follows carbon: $CO_2$ incites deep silicate melting and dehydration beneath mid-ocean ridges. *Geology* 35(2):135–138.
79. Dasgupta R, Hirschmann MM (2006) Melting in the Earth's deep upper mantle caused by carbon dioxide. *Nature* 440(7084):659–662.
80. Sharp ZD, Essene EJ, Smyth JR (1992) Ultra-high temperatures from oxygen isotope thermometry of a coesite-sanidine grospydite. *Contrib Mineral Petrol* 112:358–370.
81. Shimoda G, Tatsumi Y, Nohda S, Ishizaka K, Jahn BM (1998) Setouchi high-Mg andesites revisited: Geochemical evidence for melting of subducting sediments. *Earth Planet Sci Lett* 160:479–492.
82. Newton RC (1992) Charnockitic alteration: Evidence for $C0_2$ infiltration in granulite facies metamorphism. *J Metamorph Geol* 10:383–400.
83. Newton RC, Aranovich LY, Hansen EC, Vandenheuvel BA (1998) Hypersaline fluids in Precambrian deep-crustal metamorphism. *Precambrian Res* 91:41–63.
84. Manning CE, Aranovich LY (2014) Brines at high pressure and temperature: Thermodynamic, petrologic and geochemical effects. *Precambrian Res* 253:6–16.
85. Hilton DR, Fischer TP, Marty B (2002) Noble gases and volatile recycling at subduction zones. *Rev Mineral* 47:319–370.
86. Blundy J, Cashman KV, Rust A, Witham F (2010) A case for $CO_2$-rich arc magmas. *Earth Planet Sci Lett* 290:289–301.
87. Morner N-A, Etiope G (2002) Carbon degassing from the lithosphere. *Global Planet Change* 33:185–203.
88. Haggerty JA (1987) Petrology and geochemistry of Neogene sedimentary rocks from Mariana forearc seamounts: Implications for origin of the seamounts. *Seamounts, Islands, and Atolls*, eds Keating BH, Fryer P, Batiza R, Boehlert GW (Am Geophys Union, Washington, DC), pp 175–185.
89. Fryer P (2012) Serpentinite mud volcanism: Observations, processes, and implications. *Annu Rev Mar Sci* 4:345–373.
90. Campbell KA, Farmer JD, Des Marais D (2002) Ancient hydrocarbon seeps from the Mesozoic convergent margin of California: Carbonate geochemistry, fluids and palaeoenvironments. *Geofluids* 2:63–94.
91. Kulm LD, Suess E (1990) Relationship between carbonate deposits and fluid venting: Oregon Accretionary Prism. *J Geophys Res* 95:8899–8915.
92. Kulm LD, et al. (1986) Oregon subduction zone: Venting, fauna, and carbonates. *Science* 231(4738):561–566.
93. Sample JC (1996) Isotopic evidence from authigenic carbonates for rapid upward fluid flow in accretionary wedges. *Geology* 24:897–900.
94. Lupton J, et al. (2006) Submarine venting of liquid carbon dioxide on a Mariana Arc volcano. *Geochem Geophys Geosyst* 7(8):Q08007.
95. Sakai H, et al. (1990) Venting of carbon dioxide-rich fluid and hydrate formation in mid-Okinawa Trough backarc basin. *Science* 248(4959):1093–1096.
96. Konno U, et al. (2006) Liquid $CO_2$ venting on the seafloor: Yonaguni Knoll IV hydrothermal system, Okinawa Trough. *Geophys Res Lett* 33(16):L16607.
97. Resing JA, et al. (2009) Chemistry of hydrothermal plumes above submarine volcanoes of the Mariana Arc. *Geochem Geophys Geosyst* 10(2):Q02009.
98. Seward TM, Kerrick DM (1996) Hydrothermal CO, emission from the Taupo Volcanic Zone, New Zealand. *Earth Planet Sci Lett* 139:105–113.
99. James ER, Manga M, Rose TP, Hudson GB (2000) The use of temperature and the isotopes of O, H, C, and noble gases to determine the pattern and spatial extent of groundwater flow. *J Hydrol* 237:100–112.
100. Hacker BR, et al. (2008) Reconstruction of the Talkeetna intraoceanic arc of Alaska through thermobarometry. *J Geophys Res* 113(B3):B03204.
101. Bradshaw JY (1989) Early Cretaceous vein-related garnet granulite in Fiordland, southwest New Zealand: A case for infiltration of mantle-derived $CO_2$-rich fluids. *J Geol* 97:697–717.
102. Blattner P, Black PM (1980) Apatite and scapolite as petrogenetic indicators in granulites of Milford Sound, New Zealand. *Contrib Mineral Petrol* 74:339–348.
103. Yoshino T, Satish-Kumar M (2001) Origin of scapolite in deep-seated metagabbros of the Kohistan arc, NW Himalaya. *Contrib Mineral Petrol* 140:511–531.
104. Bouilhol P, Burg JP, Bodinier JL (2012) Gem olivine and calcite mineralization precipitated from subduction-derived fluids in the Kohistan arc-mantle (Pakistan). *Can Mineral* 50:1291–1304.
105. Bouilhol P, Burg JP, Bodinier JL, Schmidt MW (2009) Magma and fluid percolation in arc to forearc mantle: Evidence from Sapat (Kohistan, Northern Pakistan). *Lithos* 107:17–37.
106. Kelemen PB, Hanghøj K, Greene AR (2014) One view of the geochemistry of subduction-related magmatic arcs with an emphasis on primitive andesite and lower crust. *The Crust*, Treatise on Geochemistry, ed Rudnick RL (Elsevier-Pergamon, Oxford), 2nd Ed, Vol. 4, pp 749–806.
107. Jagoutz O, Schmidt M (2012) The formation and bulk composition of modern juvenile continental crust: The Kohistan arc. *Chem Geol* 298-299:79–96.
108. Houseman GA, McKenzie DP, Molnar P (1981) Convective instability of a thickened boundary layer and its relevance for the thermal evolution of continental convergent belts. *J Geophys Res* 86:6115–6132.
109. Houseman GA, Molnar P (1997) Gravitational (Rayleigh-Taylor) instability of a viscosity and convective thinning of continental layer with non-linear lithosphere. *Geophys J Int* 128:125–150.
110. Marty B, Alexander CMOD, Raymond S (2013) Primordial origins of Earth's carbon. *Rev Mineral Geochem* 75:149–181.
111. Resing JA, Lupton JE, Feely RA, Lilley MD (2004) $CO_2$ and $^3He$ in hydrothermal plumes: Implications for Mid-Ocean Ridge $CO_2$ flux. *Earth Planet Sci Lett* 226: 449–464.
112. Marty B, Tolstikhin IN (1998) $CO_2$ fluxes from mid-ocean ridges, arcs and plumes. *Chem Geol* 145:233–248.
113. Holser WT, Schidlowski M, MacKenzie FT, Maynard JB (1988) Geochemical cycles of carbon and sulfur. *Chemical Cycles in the Evolution of the Earth*, eds Gregor CB, Garrels RM, Mackenzie FT, Maynard JB (Wiley, New York), pp 105–173.
114. Wilkinson BH, Walker JCG (1989) Phanerozoic cycling of sedimentary carbonate. *Am J Sci* 289:525–548.
115. Cogley JG (1984) Continental margins and the extent and number of the continents. *Rev Geophys* 22:101–122.
116. Shirey SB, et al. (2013) Diamonds and the geology of mantle carbon. *Rev Mineral Geochem* 75:355–421.
117. Bliss JD (1992) Grade-tonnage and other models for diamond kimberlite pipes. *Nonrenewable Resour* 1:214–230.
118. Ulmer P, Trommsdorff V (1995) Serpentine stability to mantle depths and subduction-related magmatism. *Science* 268(5212):858–861.
119. Falloon TJ, Green DH (1989) The solidus of carbonated, fertile peridotite. *Earth Planet Sci Lett* 94:364–370.

# Supporting Information

## Kelemen and Manning 10.1073/pnas.1507889112

### SI Text

#### Carbon Uptake During Hydrothermal Alteration of Basaltic Oceanic Crust: More Information on $CO_2$ in Subducting Oceanic Crust

Compared with Alt and Teagle's estimates (1), [C] is now thought to be higher in volcanic rocks (2–6), and lower in gabbros of the lower crust (Dataset S1). These differences offset each other, so our estimate of about 500–600 ppm C in oceanic crust agrees with Alt and Teagle. Some data sources report averages without uncertainties, so it is difficult to assess the precision of our bulk crust estimate. Alt and Teagle proposed that continuing, off-ridge-axis alteration increases [C] in the uppermost volcanic rocks over tens of millions of years. Others propose higher carbon uptake by shallow volcanic rocks in the Cretaceous (e.g., ref. 5). However, given the scatter in published data, the significance of trends of seafloor age versus [C] in altered MORB is uncertain.

#### Carbon Uptake at the Outer Rise: Seismic Studies Indicating Serpentinization of the Mantle at the Outer Rise

For further studies, see refs. 7–11.

#### Carbon Transfer into the Leading Edge of the Mantle Wedge

**Oman Listvenites.** For additional information on Oman listvenites, see refs. 12–15.

Age data from Falk and Kelemen (11) are consistent with geologic mapping indicating that listvenites unconformably underlie late Paleocene to Eocene conglomerates (16).

In the vicinity of Wadi Mansah (619,900 m to 625,400 m east, 2,582,600 m to 2,587,150 m north, Universal Transverse Mercator coordinate system zone 40 Q), listvenite layers are enclosed entirely within peridotite, close to the basal thrust of the ophiolite (12). The basal thrust, the foliation in the peridotites, and the listvenite layers are all roughly parallel, folded in a broad anticline. We infer that the listvenites formed along imbricate faults related to the basal thrust. Several listvenite layers are present, continuous over several kilometers along strike and more than a kilometer across strike, ranging from 10 m to 200 m in thickness.

**Other Relatively Low-Temperature Listvenites.** For additional information on other relatively low-temperature listvenites, see refs. 17 and 18.

**Higher-Temperature Listvenites.** For additional information on higher-temperature listvenites, see refs. 19–23.

**High $^{87}Sr/^{86}Sr$ in Sediments Beneath the Samail Ophiolite in Oman.** For additional information on high $^{87}Sr/^{86}Sr$, see refs. 24 and 25.

**Seismic Studies of the Leading Edge of the Mantle Wedge.** Details on seismic studies are provided in Dataset S4.

***Substantial serpentine in the leading edge of the mantle wedge from seismic data.*** Seismic data are available relating to Cascadia (26–30), southern and central Japan (31–33), northern Chile (34, 35), Costa Rica (35, 36), Mariana (37–39), and Tonga (40).

***Interpretation of seismic data in terms of serpentine in the mantle wedge supported by magnetic studies.*** For an additional interpretation of seismic data, see ref. 41.

***Areas with little or no serpentine in the mantle wedge inferred from seismic data.*** Additional data are available on Hikurangi, New Zealand (42), and northeast Japan (43, 44).

#### Carbon Transfer in Greenschist and Blueschist Facies

**Carbon-Bearing Minerals and Fluids in Serpentinized Mantle Wedge Peridotites.** For additional information on carbon-bearing minerals and fluids, see refs. 19 and 45–53.

**Carbon-Bearing Minerals in Talc and/or Chlorite Schists Inferred to Be Chemically Modified Mantle Wedge Peridotites.** For additional information on carbon-bearing minerals in talc and/or chlorite schists, see refs. 54–58.

**Talc–Carbonate Lithologies Formed at ∼250–300 °C.** For additional information on talc–carbonate lithologies, see refs. 12, 21, 22, 59, and 60.

#### Carbon Transfer at High-Grade, Subsolidus Conditions

**Carbon-Bearing Minerals and Fluids in Mantle Wedge Peridotites Formed at Eclogite and UHP Facies.** Additional information is available relating to the western gneiss region of Norway (61–67), Corsica (68, 69), the eastern Alps (67, 70, 71), Bohemian peridotite massifs (72), Greece (73), and the Sulu region in China (74, 75).

**Carbonate Mineral Inclusions and Carbon-Rich Fluid Inclusions in Olivine in Peridotites from the High-Pressure Sanbagawa Belt in Southeast Japan.** For additional information on southeast Japan, see refs. 76–78.

**Higashi-Akaishi Garnet Peridotite Body and Underlying Eclogite Facies Metasediments.** For additional information on Higashi-Akaishi, see refs. 76 and 79–84.

#### Carbon Transfer in Hydrous Melts Near the Aqueous Fluid-Saturated Solidus

**Aqueous Fluid-Saturated Solidus for Metasediments and Metabasalts.** For additional information on aqueous fluid-saturated solidus, see refs. 85–90.

**Aqueous Fluid-Saturated Solidus for Metasediments and Metabasalts with Appreciable Dissolved $CO_2$.** For additional information on the presence of dissolved $CO_2$, see refs. 91–93.

#### Carbon Transfer via Fluid-Absent Melting: Fluid-Undersaturated Melting of Carbonate- and Hydrous Silicate-Bearing Compositions

Melting studies are available for carbonated peridotite with minor added $H_2O$ (review and new data in ref. 94), hydrous silicate-bearing, carbonate-bearing metabasalt (95–99), and hydrous silicate-bearing, carbonate-bearing metasediments (91–93, 100).

#### Carbon Transfer via Buoyant Diapirs

**Flux Melting of Peridotite Involving $CO_2$-Bearing Silicate Melts.** For additional information involving $CO_2$-bearing silicate melts, see refs. 101–106.

**High Degrees of Melting of Metasediments at Mantle Wedge *PT* Conditions.** For additional information on high degrees of melting, see refs. 92, 93, and 107–109.

**Shelf in the Carbonated lherzolite Solidus.** For additional information on carbonated lherzolite solidus, see refs. 110–114.

#### Diffuse Outgassing of Carbon at Forearcs and Arcs: Carbonates at Cold Seeps in Mariana Forearc

For additional information on Mariana Forearc, see refs. 115–120.

## Global Mass Balance: Critique of Outgassing Estimate of Burton et al.

A recent review by Burton et al. (121), depending heavily on Morner and Etiope (122) for diffuse fluxes, suggests that present-day, total mantle outgassing could be as high as 540 Mt C/y. This is almost 8 times higher than our upper-bound estimate of ingassing via subduction of sediments, altered oceanic crust, and serpentinized upper mantle peridotites—66 Mt C/y—and more than 4 times as high as the upper-bound estimate for subduction of 110 Mt C/y from Dasgupta and Hirschmann (102). Similarly, it is more than 4 times larger than our upper-bound estimate of 97 Mt C/y for ridge + within plate volcanic + arc volcanic + diffuse arc output, and almost 4 times greater than Dasgupta and Hirschmann's upper-bound estimate of 127 Mt C/y for outgassing. Absent some explanation for nonsteady, very high output at present, and additional evidence for the high diffuse fluxes they invoke, we infer that the estimate of Burton et al. is too high.

## Figure 3 Legend: Methods for Calculating Solubility of Carbon

Solubility of carbon was calculated for $H_2O$ in equilibrium with forsterite and enstatite. Thermodynamic data for minerals are from Holland and Powell [(123); 2002 update], for $H_2O$ and aqueous species from Sverjensky et al. (124), and for activity coefficients from Güntelberg equation (125) with $A$ parameter computed using density and dielectric constant from Sverjensky et al. (124). The dominant Ca and C species at $T < 500$ °C are $Ca^{+2}$ and $HCO_3^-$; at $T > 500$ °C, $CaHCO_3^+$ is predicted to predominate (see ref. 126). $CaCO_3$ may melt in pure $H_2O$ at $T > 800$ °C (127, 128).


1. Alt JC, Teagle DAH (1999) The uptake of carbon during alteration of oceanic crust. *Geochim Cosmochim Acta* 63:1527–1535.
2. Shilobreeva S, Martinez I, Busigny V, Agrinier P, Laverne C (2011) Insights into C and H storage in the altered oceanic crust: Results from ODP/IODP Hole 1256D. *Geochim Cosmochim Acta* 75:2237–2255.
3. Alt JC (2004) Alteration of the upper oceanic crust: Mineralogy, chemistry, and processes. *Hydrogeology of the Oceanic Lithosphere*, eds Davis EE, Elderfield H (Cambridge Univ Press, Cambridge, UK), pp 497–535.
4. Kelley KA, Plank T, Farr L, Ludden J, Staudigel H (2005) Subduction cycling of U, Th and Pb. *Earth Planet Sci Lett* 234:369–383.
5. Gillis KM, Coogan LA (2011) Secular variation in carbon uptake into the ocean crust. *Earth Planet Sci Lett* 302:385–392.
6. Coggon RM, Teagle DAH, Smith-Duque CE, Alt JC, Cooper MJ (2010) Reconstructing past seawater Mg/Ca and Sr/Ca from mid-ocean ridge flank calcium carbonate veins. *Science* 327(5969):1114–1117.
7. Ranero CR, Sallarès V (2004) Geophysical evidence for hydration of the crust and mantle of the Nazca plate during bending at the north Chile Trench. *Geology* 32:549–552.
8. Ranero CR, Morgan JP, McIntosh K, Reichert C (2003) Bending-related faulting and mantle serpentinization at the Middle America trench. *Nature* 425(6956):367–373.
9. Grevemeyer I, Ranero CR, Flueh ER, Kläschen D, Bialas J (2007) Passive and active seismological study of bending-related faulting and mantle serpentinization at the Middle America trench. *Earth Planet Sci Lett* 258:528–542.
10. Ivandic M, Grevemeyer I, Bialas J, Petersen CJ (2010) Serpentinization in the trench-outer rise region offshore of Nicaragua: Constraints from seismic refraction and wide-angle data. *Geophys J Int* 180:1253–1264.
11. Contreras-Reyes E, Grevemeyer I, Flueh ER, Reichert C (2008) Upper lithospheric structure of the subduction zone offshore of southern Arauco peninsula, Chile, at ~38°S. *J Geophys Res* 113(B7):B07303.
12. Falk ES, Kelemen PB (2015) Geochemistry and petrology of listvenite in the Somali ophiolite, Sultanate of Oman: Complete carbonation of peridotite during ophiolite emplacement. *Geochim Cosmochim Acta* 160:70–90.
13. Nasir S, et al. (2007) Mineralogical and geochemical characterization of listwaenite from the Semail ophiolite, Oman. *Chem Erde* 67:213–228.
14. Stanger G (1985) Silicified serpentinite in the Semail nappe of Oman. *Lithos* 18(1):13–22.
15. Wilde A, Simpson L, Hanna S (2002) Preliminary study of Cenozoic alteration and platinum deposition in the Oman ophiolite. *J. Virtual Explorer* 6:7–13.
16. Villey M, Le Metour J, De Gramont X (1986) *Geological Map of Fanjah* (Minist Petrol Miner, Muscat, Oman).
17. Ulrich M, et al. (2014) Dissolution–precipitation processes governing the carbonation and silicification of the serpentinite sole of the New Caledonia ophiolite. *Contrib Mineral Petrol* 167(1):952.
18. Quesnel B, et al. (2013) Syn-tectonic, meteoric water–derived carbonation of the New Caledonia peridotite nappe. *Geology* 41:1063–1066.
19. Okay AI, Harris NBW, Kelley SP (1998) Exhumation of blueschists along a Tethyan suture in northwest Turkey. *Tectonophys.* 285:275–299.
20. Borojević Šoštarić S, et al. (2014) The origin and age of the metamorphic sole from the Rogozna Mts., Western Vardar Belt: New evidence for the one-ocean model for the Balkan ophiolites. *Lithos* 192-195:39–55.
21. Beinlich A, Mavromatis V, Austrheim H, Oelkers EH (2014) Inter-mineral Mg isotope fractionation during hydrothermal ultramafic rock alteration – Implications for the global Mg-cycle. *Earth Planet Sci Lett* 392:166–176.
22. Beinlich A, Plumper O, Hovelmann J, Austrheim H, Jamtveit B (2012) Massive serpentinite carbonation at Linnajavri, N–Norway. *Terra Nova* 24:446–455.
23. Akbulut M, Piskin O, Karayigit AI (2006) The genesis of the carbonatized and silicified ultramafics known as listvenites: A case study from the Mihaliccik region (Eskisehir), NW Turkey. *Geol J* 41:557–580.
24. Weyhenmeyer CE (2000) Origin and evolution of groundwater in the alluvial aquifer of the eastern Batinah coastal plain, Sultanate of Oman: A hydrogeochemical approach. PhD dissertation (Universität Bern, Bern, Switzerland).
25. Weyhenmeyer CE, Burns SJ, Waber HN, Macumber PG, Matter A (2002) Isotope study of moisture sources, recharge areas, and groundwater flow paths within the eastern Batinah coastal plain, Sultanate of Oman. *Water Resour Res* 38(10):1184.
26. Zhao D, Rogers G, Wang K (2001) Tomographic imaging of Cascadia subduction zone in and around Vancouver Island. *Earth Planets Space* 53:285–293.
27. Bostock MG, Hyndman RD, Rondenay S, Peacock SM (2002) An inverted continental Moho and serpentinization of the forearc mantle. *Nature* 417(6888):536–538.
28. Brocher TM, Parsons R, Trehu AM, Snelson SM, Fisher MA (2003) Seismic evidence for widespread serpentinized forearc upper mantle along the Cascadia margin. *Geology* 31:267–270.
29. Ramachandran K, Doss SE, Spence GD, Hyndman RD, Brocher TM (2005) Forearc structure beneath southwestern British Columbia: A three-dimensional tomographic velocity model. *J Geophys Res* 110(B2):B02303.
30. Rondenay S, Bostock MG, Shragge J (2001) Multiparameter two-dimensional inversion of scattered teleseismic body waves: 3. Application to the Cascadia 1993 data set. *J Geophys Res* 106(B12):30795–30807.
31. Kamiya S, Kobayashi Y (2000) Seismological evidence for existence of serpentinized wedge mantle. *Geophys Res Lett* 27:819–822.
32. Xia S, Zhao D, Qiu X (2008) Tomographic evidence for the subducting oceanic crust and forearc mantle serpentinization under Kyushu, Japan. *Tectonophys* 449:85–96.
33. Kato A, et al. (2010) Variations of fluid pressure within the subducting oceanic crust and slow earthquakes. *Geophys Res Lett* 37(14):L14310.
34. Graeber FM, Asch G (1999) Three-dimensional models of *P* wave velocity and *P*-to-*S* ratio in the southern central Andes by simultaneous inversion of local earthquake data. *J Geophys Res* 104(B9):20237–20256.
35. Carlson RL, Miller DJ (2003) Mantle wedge water contents estimated from seismic velocities in partially serpentinized peridotites. *Geophys Res Lett* 30(5):1250.
36. DeShon HR, Schwartz SY (2004) Evidence for serpentinization of the forearc mantle wedge along the Nicoya Peninsula, Costa Rica. *Geophys Res Lett* 31(21):L21611.
37. Oakley AJ, Taylor B, Moore GF (2008) Pacific Plate subduction beneath the central Mariana and Izu-Bonin fore arcs: New insights from an old margin. *Geochem Geophys Geosyst* 9(6):Q06003.
38. Takahashi N, et al. (2007) Crustal structure and evolution of the Mariana intra-oceanic island arc. *Geology* 35:203–206.
39. Tibi R, Weins DA, Yuan X (2008) Seismic evidence for widespread serpentinized forearc mantle along the Mariana convergence margin. *Geophys Res Lett* 35(13):L13303.
40. Contreras-Reyes E, et al. (2011) Deep seismic structure of the Tonga subduction zone: Implications for mantle hydration, tectonic erosion, and arc magmatism. *J Geophys Res* 116(B10):B10103.
41. Blakely RJ, Brocher TM, Wells RE (2005) Subduction-zone magnetic anomalies and implications for hydrated forearc mantle. *Geology* 33:445–448.
42. Eberhart-Phillips D, Reyners M, Chadwick M, Stuart G (2008) Three-dimensional attenuation structure of the Hikurangi subduction zone in the central North Island, New Zealand. *Geophys J Int* 174:418–432.
43. Tsuji Y, Nakajima J, Hasegawa A (2008) Tomographic evidence for hydrated oceanic crust of the Pacific slab beneath northeastern Japan: Implications for water transportation in subduction zones. *Geophys Res Lett* 35(14):L14308.
44. Miura S, et al. (2005) Structural characteristics off Miyagi forearc region, the Japan Trench seismogenic zone, deduced from a wide-angle reflection and refraction study. *Tectonophysics* 407:165–188.
45. Peacock SM (1987) Serpentinization and infiltration metasomatism in the Trinity peridotite, Klamath province, northern California: Implications for subduction zones. *Contrib Mineral Petrol* 95:55–70.
46. Deschamps F, et al. (2010) In situ characterization of serpentinites from forearc mantle wedges: Timing of serpentinization and behavior of fluid-mobile elements in subduction zones. *Chem Geol* 269:262–277.
47. Deschamps F, Godard M, Guillot S, Hattori K (2013) Geochemistry of subduction zone serpentinites: A review. *Lithos* 178:96–127.
48. Guillot S, Hattori K, de Sigoyer J (2000) Mantle wedge serpentinization and exhumation of eclogites: Insights from eastern Ladakh, northwest Himalaya. *Geology* 28:199–202.
49. Guillot S, Hattori K, de Sigoyer J, Nägler T, Auzende A-L (2001) Evidence of hydration of the mantle wedge and its role in the exhumation of eclogites. *Earth Planet Sci Lett* 193:115–127.
50. Sachan HK, Mukherjee BK, Bodnar RJ (2007) Preservation of methane generated during serpentinization of upper mantle rocks: Evidence from fluid inclusions in the Nidar ophiolite, Indus Suture Zone, Ladakh (India). *Earth Planet Sci Lett* 257:47–59.
51. Vance JA, Dungan MA (1977) Formation of peridotites by deserpentinization in the Darrington and Sultan areas, Cascade Mountains, Washington. *Geol Soc Am Bull* 88: 1497–1508.

52. Johnson M, Dungan MA, Vance JA (1977) Stable isotope compositions of olivine and dolomite in peridotites formed by deserpentinization, Darrington area, North Cascades, Washington. *Geochim Cosmochim Acta* 41:431–435.
53. Brown EH, Wilson DL, Armstrong RL, Harakal JE (1982) Petrologic, structural and age relations of serpentinite, amphibolite, and blueschist in the Shuksan suite of the Iron Mountain - Gee Point area, North Cascades, Washington. *Geol Soc Am Bull* 93:1087–1098.
54. Bebout GE, Barton MD (1989) Fluid flow and metasomatism in a subduction zone hydrothermal system: Catalina Schist terrane. *Calif Geol* 17:976–980.
55. Bebout GE, Barton MD (1993) Metasomatism during subduction: Products and possible paths in the Catalina Schist, California. *Chem Geol* 108:61–92.
56. Platt JP (1975) Metamorphic and deformational processes in the Franciscan Complex, California: Some insights from the Catalina Schist terrane. *Geol Soc Am Bull* 86: 1337–1347.
57. Brovarone AV, Beyssac O (2014) Lawsonite metasomatism: A new route for water to the deep Earth. *Earth Planet Sci Lett* 393:275–284.
58. Spandler C, Hermann J, Faure K, Mavrogenes JA, Arculus RJ (2008) The importance of talc and chlorite ''hybrid'' rocks for volatile recycling through subduction zones; Evidence from the high-pressure subduction melange of New Caledonia. *Contrib Mineral Petrol* 155:181–198.
59. Hansen LD, Dipple GM, Gordon TM, Kellett DA (2005) Carbonated serpentinite (listwanite) at Atlin, British Columbia: A geological analogue to carbon dioxide sequestration. *Can Mineral* 43:225–239.
60. Schandl ES, Wicks FJ (1991) Carbonate and associated alteration of ultramafic and rhyolitic rocks at the Hemingway Property, Kidd Creek Volcanic Complex, Timmins, Ontario. *Econ Geol* 88:1615–1635.
61. Malvoisin B, Chopin C, Brunet F, Galvez ME (2012) Low-temperature wollastonite formed by carbonate reduction: A marker of serpentinite redox conditions. *J Petrol* 53:159–176.
62. Vrijmoed JC, Roermund HLMV, Davies GR (2006) Evidence for diamond-grade ultrahigh pressure metamorphism and fluid interaction in the Svartberget Fe–Ti garnet peridotite–websterite body, Western Gneiss Region, Norway. *Mineral Petrol* 88: 381–405.
63. van Roermund HLM (2009) Mantle-wedge garnet peridotites from the northernmost ultra-high pressure domain of the Western Gneiss Region, SW Norway. *Eur J Mineral* 21:1085–1096.
64. Brueckner HK, Carswell DA, Griffin WL (2002) Paleozoic diamonds within a Precambrian peridotite lens in UHP gneisses of the Norwegian Caledonides. *Earth Planet Sci Lett* 203(3-4):805–816.
65. van Roermund HLM, Carswell DA, Drury MR, Heijboer TC (2002) Microdiamonds in a megacrystic garnet websterite pod from Bardane on the island of Fjørtoft, western Norway: Evidence for diamond formation in mantle rocks during deep continental subduction. *Geology* 30:959–962.
66. Carswell DA, van Roermund HLM (2005) On multi-phase mineral inclusions associated with microdiamond formation in mantle-derived peridotite lens at Bardane on Fjørtoft, west Norway. *Eur J Mineral* 17:31–42.
67. Scambelluri M, van Roermund HLM, Pettke T (2010) Mantle wedge peridotites: Fossil reservoirs of deep subduction zone processes: Inferences from high and ultrahigh-pressure rocks from Bardane (Western Norway) and Ulten (Italian Alps). *Lithos* 120: 186–201.
68. Galvez ME, et al. (2013) Metasomatism and graphite formation at a lithological interface in Malaspina (Alpine Corsica, France). *Contrib Mineral Petrol* 166: 1687–1708.
69. Galvez ME, et al. (2013) Graphite formation by carbonate reduction during subduction. *Nat Geosci* 6:473–477.
70. Sapienza GT, Scambelluri M, Braga R (2009) Dolomite-bearing orogenic garnet peridotites witness fluid-mediated carbon recycling in a mantle wedge (Ulten Zone, Eastern Alps, Italy). *Contrib Mineral Petrol* 158:401–420.
71. Zanetti A, Mazzucchelli M, Rivalenti G, Vannucci R (1999) The Finero phlogopite-peridotite massif: An example of subduction-related metasomatism. *Contrib Mineral Petrol* 134:107–122.
72. Naemura K, Hirajima T, Svotka M (2009) The pressure-temperature path and the origin of phlogopite in spinel-garnet peridotites from the Blansky Les Massif of the Moldanubian Zone, Czech Republic. *J Petrol* 50:1795–1827.
73. Ague JJ, Nicolescu S (2014) Carbon dioxide released from subduction zones by fluid-mediated reactions. *Nat Geosci* 7:355–360.
74. Zhang RY, Yang JS, Wooden JL, Liou JG, Li TF (2005) U--Pb SHRIMP geochronology of zircon in garnet peridotite from the Sulu UHP terrane, China: Implications for mantle metasomatism and subduction-zone UHP metamorphism. *Earth Planet Sci Lett* 237: 729–743.
75. Zhang RY, et al. (2007) Multiple metasomatism in Sulu ultrahigh-P garnet peridotite constrained by petrological and geochemical investigations. *J Metamorph Geol* 25: 149–164.
76. Enami M, Mizukami T, Yokoyama K (2004) Metamorphic evolution of garnet-bearing ultramafic rocks from the Gongen area, Sanbagawa belt, Japan. *J Metamorph Geol* 22:1–15.
77. Hirai H, Arai S (1987) $H_2O$-$CO_2$ fluids supplied in alpine-type mantle peridotites: Electron petrology of relic fluid inclusions in olivines. *Earth Planet Sci Lett* 85: 311–318.
78. Arai S, Ishimaru S, Mizukami T (2012) Methane and propane micro-inclusions in olivine in titanoclinohumite bearing dunites from the Sanbagawa high-P metamorphic belt, Japan: Hydrocarbon activity in a subduction zone and Ti mobility. *Earth Planet Sci Lett* 353-354:1–11.
79. Miyamoto A, Enami M, Tsuboi M, Yokoyama K (2007) Peak conditions of kyanite-bearing quartz eclogites in the Sanbagawa metamorphic belt, central Shikoku, Japan. *J Mineral Petrol Sci* 102:352–367.
80. Aoya M, Endo S, Mizukami T, Wallis SR (2013) Paleo-mantle wedge preserved in the Sambagawa high-pressure metamorphic belt and the thickness of forearc continental crust. *Geology* 41:451–454.
81. Mizukami T, Wallis SR (2005) Structural and petrological constraints on the tectonic evolution of the garnet-lherzolite facies Higashi-Akaishi peridotite body, Sanbagawa belt, SW Japan. *Tectonics* 24(6):TC6012.
82. Endo S, Tsuboi M (2013) Petrogenesis and implications of jadeite-bearing kyanite eclogite from the Sanbagawa belt (SW Japan). *J Metamorph Geol* 31:647–661.
83. Uno M, et al. (2014) Elemental transport upon hydration of basic schists during regional metamorphism: Geochemical evidence from the Sanbagawa metamorphic belt, Japan. *Geochem J* 48:29–49.
84. Banno S (2004) Ultramafic rocks and associated eclogites of the Sanbagawa schists, Japan: A review. *Int Geol Rev* 46:693–704.
85. Hermann J (2002) Experimental constraints on phase relations in subducted continental crust. *Contrib Mineral Petrol* 143:219–235.
86. Hermann J, Green DH (2001) Experimental constraints on high pressure melting in subducted crust. *Earth Planet Sci Lett* 188:149–168.
87. Hermann J, Spandler CJ (2008) Sediment melts at sub-arc depths: An experimental study. *J Petrol* 49:717–740.
88. Schmidt MW, Vielzeuf D, Auzanneau E (2004) Melting and dissolution of subducting crust at high pressures: The key role of white mica. *Earth Planet Sci Lett* 228:65–84.
89. Nichols GT, Wyllie PJ, Stern CR (1994) Subduction zone melting of pelagic sediments constrained by melting experiments. *Nature* 371:785–788.
90. Skora S, Blundy J (2010) High-pressure hydrous phase relations of radiolarian clay and implications for the involvement of subducted sediment in arc magmatism. *J Petrol* 51:2211–2243.
91. Thomsen TB, Schmidt MW (2008) The biotite to phengite reaction and mica-dominated melting in fluid carbonate-saturated pelites at high pressures. *J Petrol* 49: 1889–1914.
92. Tsuno K, Dasgupta R (2011) Melting phase relation of nominally anhydrous, carbonated pelitic-eclogite at 2.5–3.0 GPa and deep cycling of sedimentary carbon. *Contrib Mineral Petrol* 161:743–763.
93. Tsuno K, Dasgupta R, Danielson L, Righter K (2012) Flux of carbonate melt from deeply subducted pelitic sediments: Geophysical and geochemical implications for the source of Central American volcanic arc. *Geophys Res Lett* 39(16):L16307.
94. Tumiati S, Fumaga P, Tiraboschi C, Poli S (2013) An experimental study on COH-bearing peridotite up to 3.2 GPa and implications for crust-mantle recycling. *J Petrol* 54:453–479.
95. Kiseeva ES, et al. (2012) An experimental study of carbonated eclogite at 3.5-5.5 GPa—Implications for silicate and carbonate metasomatism in the cratonic mantle. *J Petrol* 53:727–759.
96. Gerbode C, Dasgupta R (2010) Carbonate-fluxed melting of MORB-like pyroxenite at 2.9 GPa and genesis of HIMU ocean island basalts. *J Petrol* 51:2067–2088.
97. Yaxley GM, Green DH (1994) Experimental demonstration of refractory carbonate-bearing eclogite and siliceous melt in the subduction regime. *Earth Planet Sci Lett* 128:313–325.
98. Dasgupta R, Hirschmann MM, Dellas N (2005) The effect of bulk composition on the solidus of carbonated eclogite from partial melting experiments at 3 GPa. *Contrib Mineral Petrol* 149:288–305.
99. Dasgupta R, Hirschmann MM, Withers AC (2004) Deep global cycling of carbon constrained by the solidus of anhydrous, carbonated eclogite under upper mantle conditions. *Earth Planet Sci Lett* 227:73–85.
100. Grassi D, Schmidt MW (2011) Melting of carbonated pelites at 8–13 GPa: Generating K-rich carbonatites for mantle metasomatism. *Contrib Mineral Petrol* 162(1): 169–191.
101. Dasgupta R, Hirschmann MM, Smith ND (2007) Water follows carbon: $CO_2$ incites deep silicate melting and dehydration beneath mid-ocean ridges. *Geology* 35: 135–138.
102. Dasgupta R, Hirschmann MM (2010) The deep carbon cycle and melting in Earth's interior. *Earth Planet Sci Lett* 298:1–13.
103. Mallik A, Dasgupta R (2013) Reactive infiltration of MORB-eclogite-derived carbonated silicate melt into fertile peridotite at 3 GPa and genesis of alkalic magmas. *J Petrol* 53:2267–2300.
104. Mallik A, Dasgupta R (2012) Reaction between MORB-eclogite derived melts and fertile peridotite and generation of ocean island basalts. *Earth Planet Sci Lett* 329-330:97–108.
105. Mallik A, Dasgupta R (2014) Effect of variable $CO_2$ on eclogite-derived andesite and lherzolite reaction at 3 GPa—Implications for mantle source characteristics of alkalic ocean island basalts. *Geochem Geophys Geosyst* 15:1533–1557.
106. Duncan MS, Dasgupta R (2014) $CO_2$ solubility and speciation in rhyolitic sediment partial melts at 1.5–3.0 GPa – Implications for carbon flux in subduction zones. *Geochim Cosmochim Acta* 124:328–347.
107. Behn MD, Kelemen PB, Hirth G, Hacker BR, Massonne HJ (2011) Diapirs as the source of the sediment signature in arc lavas. *Nat Geosci* 4(9):641–646.
108. Kelemen PB, Hanghøj K, Greene A (2003) One view of the geochemistry of subduction-related magmatic arcs, with an emphasis on primitive andesite and lower crust. *The Crust*, Treatise on Geochemistry, ed Rudnick RL (Elsevier-Pergamon, Oxford), Vol 3, pp 593–659.
109. Spandler C, Yaxley G, Green DH, Scott D (2010) Experimental phase and melting relations of metapelite in the upper mantle: implications for the petrogenesis of intraplate magmas. *Contrib Mineral Petrol* 160:569–589.
110. Ellis DE, Wyllie PJ (1980) Phase relations and their petrological implications in the system MgO-$SiO_2$-$H_2O$-$CO_2$ at pressures up to 100 kbar. *Am Mineral* 65:540–556.

111. Wyllie PJ, Huang W-L (1976) Carbonation and melting reactions in the system CaO-MgO-$SiO_2$-$CO_2$ at mantle pressures with geophysical and petrological applications. *Contrib Mineral Petrol* 54:79–107.
112. Falloon TJ, Green DH (1990) Solidus of carbonated fertile peridotite under fluid-saturated conditions. *Geology* 18:195–199.
113. Falloon TJ, Green DH (1989) The solidus of carbonated, fertile peridotite. *Earth Planet Sci Lett* 94:364–370.
114. Eggler DH (1978) The effect of $CO_2$ upon partial melting of peridotite in the system $Na_2O$-CaO-$Al_2O_3$-MgO-$SiO_2$-$CO_2$ to 35 kbar, with an analysis of melting in a peridotite-$H_2O$-$CO_2$ system. *Am J Sci* 278:305–343.
115. Haggerty JA (1987) Petrology and geochemistry of Neogene sedimentary rocks from Mariana forearc seamounts: Implications for origin of the seamounts. *Seamounts, Islands, and Atolls*, eds Keating BH, Fryer P, Batiza R, Boehlert GW (Am Geophys Union, Washington, DC), pp 175–185.
116. Haggerty JA (1991) Evidence from fluid seeps atop serpentine seamounts in the Mariana Forearc: Clues for emplacement of the seamounts and their relationship to forearc tectonics. *Mar Geol* 102:293–309.
117. Haggerty JA, Chaudhuri S (1992) Strontium isotopic composition of the interstitial waters from Leg 125: Mariana and Bonin forearcs. *Proc Ocean Drill Program Sci Results* 125:397–400. Available at www-odp.tamu.edu/publications/citations/cite125.html. Accessed May 17, 2015.
118. Fryer P, et al. (1990) Conical Seamount: SeaMARC II, Alvin submersible, and seismic reflection studies. *Proc Ocean Drill Program Initial Rep* 125:69–80. Available at www-odp.tamu.edu/publications/citations/cite125.html. Accessed May 17, 2015.
119. Fryer P, Wheat CG, Mottl MJ (1999) Mariana Blueschist mud volcanism: Implications for conditions within the subduction zone. *Geology* 27:103–106.
120. Fryer P, Gharib J, Ross K, Savov I, Mottl MJ (2006) Variability in serpentinite mudflow mechanisms and sources: ODP drilling results on Mariana forearc seamounts. *Geochem Geophys Geosyst* 7(8):Q08014.
121. Burton MR, Sawyer GM, Granieri D (2013) Deep carbon emissions from volcanoes. *Rev Mineral Geochem* 75:323–354.
122. Morner N-A, Etiope G (2002) Carbon degassing from the lithosphere. *Global Planet Change* 33:185–203.
123. Holland TJB, Powell R (1998) An internally consistent thermodynamic data set for phases of petrological interest. *J Metamorph Geol* 16:309–343. 2002 update available at www.esc.cam.ac.uk/research/research-groups/holland/thermocalc. Accessed May 17, 2015.
124. Sverjensky DA, Harrison B, Azzolini D (2014) Water in the deep Earth: The dielectric constant and the solubilities of quartz and corundum to 60kb and 1200° C. *Geochim Cosmochim Acta* 129:125–145.
125. Manning CE (2013) Thermodynamic modeling of fluid-rock interaction at mid-crustal to upper mantle conditions. *Rev Mineral Geochem* 76:135–164.
126. Facq S, Daniel I, Montagnac G, Cardon H, Sverjensky DA (2014) In situ Raman study and thermodynamic model of aqueous carbonate speciation in equilibrium with aragonite under subduction zone conditions. *Geochim Cosmochim Acta* 132:375–390.
127. Wyllie PJ, Tuttle OF (1960) The system CaO-$CO_2$-$H_2O$ and the origin of carbonatites. *J Petrol* 1:1–46.
128. Caciagli NC, Manning CE (2003) The solubility of calcite in water at 6–16 kbar and 500–800 °C. *Contrib Mineral Petrol* 146:275–285.

**Dataset S1. Compiled data on carbon concentration in the oceanic crust, an update of the classic study of Alt and Teagle (1) incorporating newer data. Data sources are refs. 2–11**

Dataset S1

1. Alt JC, Teagle DAH (1999) The uptake of carbon during alteration of oceanic crust. *Geochim Cosmochim Acta* 63:1527–1535.
2. Shilobreeva S, Martinez I, Busigny V, Agrinier P, Laverne C (2011) Insights into C and H storage in the altered oceanic crust: Results from ODP/IODP Hole 1256D. *Geochim Cosmochim Acta* 75:2237–2255.
3. Gillis KM, Coogan LA (2011) Secular variation in carbon uptake into the ocean crust. *Earth Planet Sci Lett* 302:385–392.
4. Dick HJB, et al. (1999) *Proceedings of the Ocean Drilling Program, Initial Reports* (Ocean Drilling Program, College Station, TX), Vol 176.
5. Fruh-Green GL, Connolly JAD, Plas A (2004) Serpentinization of oceanic peridotites: Implications for geochemical cycles and biological activity. *The Subseafloor Biosphere at Mid-Ocean Ridges*, eds Wilcock WSD, et al. (Am Geophys Union, Washington, DC), pp 119–136.
6. Gillis KM, et al. (1993) *Proceedings of the Ocean Drilling Program, Initial Reports* (Ocean Drilling Program, College Station, TX), Vol 147.
7. Cannat M, et al. (1995) *Proceedings of the Ocean Drilling Program, Initial Reports* (Ocean Drilling Program, College Station, TX), Vol 153.
8. Kelemen PB, et al. (2004) *Proceedings of the Ocean Drilling Program, Initial Reports* (Ocean Drilling Program, College Station, TX), Vol 209.
9. Blackman DK, et al. (2006) *Proceedings of the Integrated Ocean Drilling Program* (Ocean Drilling Program, College Station, TX), Vol 304-305.
10. Coggon RM (2006) Hydrothermal alteration of the ocean crust: Insights from Macquarie Island and drilled in situ ocean crust. PhD dissertation (University of Southampton, Southampton, UK).
11. Kelemen PB, et al. (2011) Rates and mechanisms of mineral carbonation in peridotite: Natural processes and recipes for enhanced, in situ $CO_2$ capture and storage. *Annu Rev Earth Planet Sci* 39:545–576.

**Dataset S2. Compiled data on carbon concentration in abyssal peridotites dredged and drilled from the midocean ridges, and in peridotites from the mantle section of ophiolites. Most analyses are by total combustion, and the results are reported in terms of total carbon as $CO_2$. Data sources are our new data on Oman ophiolite mantle peridotites (Dataset S5) and refs. 1–6**

Dataset S2

1. Fruh-Green GL, Connolly JAD, Plas A (2004) Serpentinization of oceanic peridotites: Implications for geochemical cycles and biological activity. *The Subseafloor Biosphere at Mid-Ocean Ridges*, eds Wilcock WSD, et al. (Am Geophys Union, Washington, DC), pp 119–136.
2. Gillis KM, et al. (1993) *Proceedings of the Ocean Drilling Program, Initial Reports* (Ocean Drilling Program, College Station, TX), Vol 147.
3. Cannat M, et al. (1995) *Proceedings of the Ocean Drilling Program, Initial Reports* (Ocean Drilling Program, College Station, TX), Vol 153.
4. Kelemen PB, et al. (2004) *Proceedings of the Ocean Drilling Program, Initial Reports* (Ocean Drilling Program, College Station, TX), Vol 209.
5. Coggon RM (2006) Hydrothermal alteration of the ocean crust: Insights from Macquarie Island and drilled in situ ocean crust. PhD dissertation (University of Southampton, Southampton, UK).
6. Delacour A, Früh-Green GL, Bernasconi SM, Schaeffer P, Kelley DS (2008) Carbon geochemistry of serpentinites in the Lost City hydrothermal system (30°N, MAR). *Geochim Cosmochim Acta* 72:3681–3702.

**Dataset S3. Summary of carbon flux estimates discussed throughout this paper**

Dataset S3

**Dataset S4. Compiled estimates of the proportion of serpentine and volume of serpentinized peridotite in forearc mantle wedges inferred from seismic studies. Data sources are refs. 1–19**

Dataset S4


1. Zhao D, Rogers G, Wang K (2001) Tomographic imaging of Cascadia subduction zone in and around Vancouver Island. *Earth Planets Space* 53:285–293.
2. Bostock MG, Hyndman RD, Rondenay S, Peacock SM (2002) An inverted continental Moho and serpentinization of the forearc mantle. *Nature* 417(6888):536–538.
3. Brocher TM, Parsons R, Trehu AM, Snelson SM, Fisher MA (2003) Seismic evidence for widespread serpentinized forearc upper mantle along the Cascadia margin. *Geology* 31:267–270.
4. Ramachandran K, Doss SE, Spence GD, Hyndman RD, Brocher TM (2005) Forearc structure beneath southwestern British Columbia: A three-dimensional tomographic velocity model. *J Geophys Res* 110(B2):B02303.
5. Rondenay S, Bostock MG, Shragge J (2001) Multiparameter two-dimensional inversion of scattered teleseismic body waves: 3. Application to the Cascadia 1993 data set. *J Geophys Res* 106(B12):30795–30807.
6. Kamiya S, Kobayashi Y (2000) Seismological evidence for existence of serpentinized wedge mantle. *Geophys Res Lett* 27:819–822.
7. Xia S, Zhao D, Qiu X (2008) Tomographic evidence for the subducting oceanic crust and forearc mantle serpentinization under Kyushu, Japan. *Tectonophys.* 449:85–96.
8. Kato A, et al. (2010) Variations of fluid pressure within the subducting oceanic crust and slow earthquakes. *Geophys Res Lett* 37(14):L14310.
9. Graeber FM, Asch G (1999) Three-dimensional models of *P* wave velocity and *P*-to-*S* ratio in the southern central Andes by simultaneous inversion of local earthquake data. *J Geophys Res* 104(B9):20237–20256.
10. Carlson RL, Miller DJ (2003) Mantle wedge water contents estimated from seismic velocities in partially serpentinized peridotites. *Geophys Res Lett* 30(5):1250.
11. DeShon HR, Schwartz SY (2004) Evidence for serpentinization of the forearc mantle wedge along the Nicoya Peninsula, Costa Rica. *Geophys Res Lett* 31(21):L21611.
12. Oakley AJ, Taylor B, Moore GF (2008) Pacific Plate subduction beneath the central Mariana and Izu-Bonin fore arcs: New insights from an old margin. *G-cubed* 9(6):Q06003.
13. Takahashi N, et al. (2007) Crustal structure and evolution of the Mariana intra-oceanic island arc. *Geology* 35:203–206.
14. Tibi R, Weins DA, Yuan X (2008) Seismic evidence for widespread serpentinized forearc mantle along the Mariana convergence margin. *Geophys Res Lett* 35(13):L13303.
15. Contreras-Reyes E, et al. (2011) Deep seismic structure of the Tonga subduction zone: Implications for mantle hydration, tectonic erosion, and arc magmatism. *J Geophys Res* 116(B10): B10103.
16. Eberhart-Phillips D, Reyners M, Chadwick M, Stuart G (2008) Three-dimensional attenuation structure of the Hikurangi subduction zone in the central North Island, New Zealand. *Geophys J Int* 174:418–432.
17. Tsuji Y, Nakajima J, Hasegawa A (2008) Tomographic evidence for hydrated oceanic crust of the Pacific slab beneath northeastern Japan: Implications for water transportation in subduction zones. *Geophys Res Lett* 35(14):L14308.
18. Miura S, et al. (2005) Structural characteristics off Miyagi forearc region, the Japan Trench seismogenic zone, deduced from a wide-angle reflection and refraction study. *Tectonophysics* 407:165–188.
19. Wada I, Wang K (2009) Common depth of slab-mantle decoupling: Reconciling diversity and uniformity of subduction zones. *Geochem Geophys Geosyst* 10(10):Q10009.


**Dataset S5. Our new analyses of partially serpentinized peridotites from the Samail ophiolite in Oman (1), together with analyses of previously analyzed samples of partially serpentinized peridotite from the Northern Apennine ophiolite (2)**

Dataset S5


1. Hanghøj K, Kelemen PB, Hassler D, Godard M (2010) Composition and genesis of depleted mantle peridotites from the Wadi Tayin massif, Oman ophiolite: Major and trace element geochemistry, and Os isotope and PGE systematics. *J Petrol* 51:206–227.
2. Schwarzenbach EM, Früh-Green GL, Bernasconi SM, Alt JC, Plas A (2013) Serpentinization and carbon sequestration: A study of two ancient peridotite-hosted hydrothermal systems. *Chem Geol* 351:115–133.